3-9168

UNIVERSITY OF TORONTO

NUMERICAL SIMULATION

OF

STEAM INJECTION IN BITUMEN

AND HEAVY OIL RESERVOIRS

PHASE 1: PART 1

OST 83-00195

DEPARTMENT OF CHEMICAL ENGINEERING
AND APPLIED CHEMISTRY

UNIVERSITY OF TORONTO
TORONTO, CANADA M5S 1A4

DEPARTMENT OF CHEMICAL ENGINEERING
AND APPLIED CHEMISTRY

February 5, 1987.

Dr. Albert E. George,
Energy Research Laboratories,
CANMET,
555 Booth Street,
Ottawa, Ontario.
K1A 0G1

Dear Albert:

Please find enclosed a copy of Part I of the final report on Phase I.

Yours sincerely,

Donald E. Cormack
Associate Professor

DEC:pb

Enclosure

89PP.

NUMERICAL SIMULATION

OF

STEAM INJECTION IN BITUMEN

AND HEAVY OIL RESERVOIRS

PHASE 1: PART 1

Prepared for

The Department of Energy Mines and Resources, Canada

under contract OST83-00195

22ST•23440-3-9168

MICROMEDIA

This document was produced by scanning the original publication.
Ce document est le produit d'une numérisation par balayage de la publication originale.
(CANMET)

by

Peter G. DeBuda

and

Donald E. Cormack

Department of Chemical Engineering and Applied Chemistry

University of Toronto

89pp

ABSTRACT

A sequential, iterative, fully implicit, one-dimensional, steamflood simulator is presented. The technique effectively divides the governing equations into two groups, which are iteratively solved in a sequential manner at each time step. It is shown that mass and energy balance errors can be maintained at extremely small levels using this technique.

It is demonstrated in theory that for three-dimensional simulations of systems with several oil components, the sequential method potentially offers significant savings in computation time. However, this optimism is tempered with the observation that certain techniques which were used to speed the convergence of the one-dimensional simulator are likely to be considerably less successful in two and three dimensions.

In the second part of the report, a procedure is presented by which the location of the steam front can be tracked with the purpose of improving the accuracy of the simulator. The velocity of the steam front, and several state variables at the steam front, are solved for directly from the governing equations. It is demonstrated that the front-tracking technique is able to reduce considerably spurious oscillations in state variables and injection rates as the steam front advances through the computational grid. Furthermore, evidence suggests that the front-tracking technique displays smaller truncation errors than does the method without front-tracking.

1. INTRODUCTION

Numerical simulation plays an important role in the design and optimization of almost all oil recovery schemes, whether the recovery be

primary, secondary or enhanced. As the sophistication and cost of the recovery effort increases, even greater emphasis is placed on numerical simulation studies. This is particularly so when thermal recovery methods, such as steam injection and in situ combustion, are used.

It has recently become standard practice to employ a numerical formulation which is referred to as "highly implicit" (c.f. Coats[1]). In this procedure, all governing equations, which include transport equations and equilibrium relationships, are handled simultaneously. The finite-difference formulation of the equations is stepped ahead in time by means of an iterative, Newton linearization procedure. Another approach to the thermal simulation problem is one in which not all dependent variables are solved for simultaneously. Instead, the governing equations are segregated into groups, and the groups are solved "sequentially"[2-8].

The general tendency for simulators to shift from sequential solution techniques to the strongly implicit, simultaneous solution technique has been motivated by the notion that the sequential methods are less reliable, in that stability problems may arise during a simulation, and that they give rise to unacceptably larger numerical errors (i.e., mass and energy balance errors). This view has been prominently voiced by Coats[1]. On the other hand, sequential methods involve significantly less computer memory and could potentially require considerably less computer time than the simultaneous methods, if the above perceived problems could be overcome.

Another problem, which plagues essentially all steam injection numerical simulators which have been presented in the literature, is spurious injection pressure oscillations in time. Figure 1.1 demonstrates the nature of the problem for steam injection into a core at constant injection rate. The large

Figure 1.1 Injection pressure oscillations generated by standard finite-difference numerical steam-flood simulator - one-dimensional flow (from Vinsome [9])

oscillations in pressure are observed to be correlated with the movement of the steam front past each grid point in the finite-difference grid. When injection is carried out at constant pressure, large oscillations in injection rate (variations by a factor of three) are observed in the simulated results. The reliability of numerical simulators which are subject to such spurious behaviour must be questioned.

In the first part of the present report, a new iterative, sequential simulation procedure, which is a modified version of the method described by Beattie[7], is presented. The primary emphasis of this work is to obtain a more rapid solution of the governing equations in a shorter computation time than is required for the fully implicit methods, without compromising the stability and accuracy of the solution. Techniques have been developed which improve the convergence characteristics of the simulator. Evidence indicates that for two- and three-dimensional multicomponent systems, substantial savings in computer time can potentially be achieved with this method.

In the second part of the report, a technique to track the position of the steam front during steam injection is presented. In addition to determining the location of the steam front, the model equations allow the calculation of several state variables at the steam front. It is shown that, by including the front-tracking procedure in the simulator, the spurious variations in pressure or injection rate can be reduced considerably.

2. THE NUMERICAL SIMULATOR WITHOUT FRONT-TRACKING

2.1 The Governing Equations

The continuum partial differential equations which govern the flow of steam, oil, water and gas through a porous medium are well known. They can be

represented in finite-difference form, for one-dimensional flow, as (variables are defined in the nomenclature at the end of the report)

(i) C+1 component mole balances

$$\frac{1}{\delta t}\,\delta(\phi S_p \rho_p w_i)_j^n = \frac{1}{X_{j+\frac{1}{2}} - X_{j-\frac{1}{2}}}\,\Delta_X(T_p w_i \Delta_X P)_j^n + \sigma_p (M_i)_j^n ,$$

$$j=1,\ldots,N \quad , \qquad i=1,\ldots,C+1 \quad , \quad p=g,w,o \tag{2.1}$$

(ii) the enthalpy balance

$$\frac{1}{\delta t}\,\delta\Big(\phi \sum_p S_p \rho_p h_p + (1-\phi)\rho_r h_r\Big)_j^n = \frac{1}{X_{j+\frac{1}{2}} - X_{j-\frac{1}{2}}}\,\Delta_X\Big(\sum_p T_p h_p \Delta_X P\Big)_j^n + \frac{1}{X_{j+\frac{1}{2}} - X_{j-\frac{1}{2}}}\,\Delta_X(T_c \Delta_X T)_j^n - (q_L)_j^n , \qquad j=1,..,N \tag{2.2}$$

where the difference operators are defined as

$$\delta(\xi)_j^n \equiv (\xi)_j^n - (\xi)_j^{n-1} \tag{2.3}$$

and

$$\Delta_X(T\eta\Delta_X\xi)^n_j \equiv (T\eta)^n_{j+\frac{1}{2}}(\xi^n_{j+1}-\xi^n_j) - (T\eta)^n_{j-\frac{1}{2}}(\xi^n_j-\xi^n_{j-1}) \qquad (2.4)$$

In addition to equations (2.1) and (2.2), several algebraic constraints must be satisfied. These include the phase saturation constraint,

$$\sum_{p=1}^{3} S_p = 1 \ , \qquad (2.5)$$

the mole fraction constraint,

$$\sum_{i=1}^{C} x_i = 1 \ , \qquad (2.6)$$

and, at points where vapour is present,

$$\sum_{i=1}^{C+1} y_i = 1 \qquad (2.7)$$

where
$$y_{C+1} = p_s(T)/P$$

and
$$y_i = x_i p_i(T)/P \ , \ i=1,\ldots,C \qquad (2.8)$$

(If the subscript i is between 1 and C inclusive, it refers to an oil-phase

component; if i = C+1, it refers to the water.) The functions $p_i(T)$ and $p_s(T)$ are the pure component vapour pressures of oil component i and steam respectively. The equations for the secondary variables (i.e. densities, viscosities, enthalpies, relative permeabilities, transmissibilities, mobilities, vapour pressures, porosity and thermal conductivity) in terms of the primary variables, (i.e. temperature, pressure, saturations and compositions) are given in the appendix, for the test case considered in the present work.

In the present work, it was intended that the simulation represent the flow of steam from a vertical fracture into the oil-bearing formation. For this purpose, the commonly used constant injection rate boundary condition[1,8,9] is not appropriate. Instead, it is more appropriate to specify the fracture-face pressure P(0,t), and (if a liquid phase is being injected along with the steam) the ratios of phase injection rates

$$J_p(t) = \frac{q_p(0,t)}{q_T(0,t)} \ , \ p=1,\ldots,3 \qquad (2.9)$$

If the composition of the liquid hydrocarbon at the boundary, $x_i(0,t)$, is known at a given time, then the boundary value of the temperature can be calculated by means of the Newton-Raphson iteration procedure applied to equation (2.7), together with the vapour pressure expressions in the appendix, and the specified boundary pressure. Likewise, the boundary values of the saturations S_p, p=1,...,3, can be calculated by means of the Newton-Raphson iteration procedure applied to equation (2.9), together with the mobility expressions in the appendix, and the calculated temperature. Thus, the

boundary values $T(0,t)$ and $S_p(0,t)$ may be treated as secondary variables (together with viscosities, etc.) On the other hand, the boundary hydrocarbon compositions, $x_i(0,t)$, and the total volumetric injection rate $q_T(0,t)$ must be treated as primary variables, and hence obtained by solving the combined governing equations and boundary conditions.

At the $X=X_{max}$ boundary, the following conditions were imposed.

$$P(X_{max},t) \text{ is specified} \tag{2.10}$$

and

$$\frac{\partial^2 T}{\partial X^2}(X_{max},t) = 0 \tag{2.11}$$

(The boundary condition (2.11) is based on the assumption that the conductive heat flux does not vary with position near the $X=X_{max}$ boundary. The question as to whether this boundary condition is appropriate requires further study. However, it is the least inappropriate condition among several that could be considered.)

In discretized form, the above boundary conditions can be summarized as:

$$P_1^n,\ P_N^n \qquad \text{specified} \tag{2.12}$$

and

$$T_{N+1}^n = 2T_N^n - T_{N-1}^n \tag{2.13}$$

where T_{N+1}^n is the temperature at the fictitious point

$$X_{N+1} = 2X_N - X_{N-1} \tag{2.14}$$

To accommodate the boundary condition (2.9), the expression $\Delta_X(T\eta\Delta_X\xi)_1^n$ is redefined as

$$\Delta_X(T\eta\Delta_X\xi)_1^n \equiv (T\eta)_{1\frac{1}{2}}^n(\xi_2^n-\xi_1^n) + (J_p)_1^n(q_T\rho_p\eta)_1^n \tag{2.15}$$

where $(J_p)_1^n$ is specified and $(q_T)_1^n$, the total volumetric injection rate, is a new unknown. In a similar manner, since one of the terms in equation (2.4) is not defined when j = N, the expression $\Delta_X(T\eta\Delta_X\xi)_N^n$ is redefined as

$$\Delta_X(T\eta\Delta_X\xi)_N^n \equiv -(T\eta)_{N-\frac{1}{2}}^n(\xi_N^n-\xi_{N-1}^n) - \left(\frac{q_T\tau_p\eta}{\Sigma_p\tau_p/\rho_p}\right)_N^n \tag{2.16}$$

2.2 The Two-level Iterative Method

The proposed iterative method is based on the idea of splitting both the variables and the equations into two groups as given in table 2.1. This method is described in figure 2.1, where $\underline{U}_{PT}$, $\underline{U}_{SX}$, $\underline{F}_{PT}$, $\underline{F}_{SX}$ denote the vectors of the PT unknowns, the SX unknowns, the PT equations, and the SX equations respectively. After initial guesses are made for the values of all unknowns at time step n, one step of the Newton-Raphson method is applied to the PT equations in order to obtain improved estimates of the PT unknowns. Next,

one step of the Newton-Raphson method is applied to the SX equations in order to obtain improved estimates of the SX unknowns. This procedure is repeated until convergence is attained.

The proposed method can be thought of as an IMPES-like* procedure, with iterative improvement, wherein saturations calculated for time step n are used to calculate improved values for pressures and temperatures, and vice versa. However, this method differs from other IMPES methods in that, during the iteration process, the gas saturations, S_g, are grouped with the temperatures and pressures rather than with the other saturations and compositions. This approach was suggested by Coats[1], but was criticized in the same article and was apparently not pursued further by him.

2.3 The PT Equations

In the standard IMPES method, the mole balances for each phase are divided by the phase molar density, and then are added together in order to eliminate the saturation terms. Since, in the present model, the oil phase has more than one component, it is better (for the convergence of the iteration procedure) to divide each component-phase mole balance (2.1) by the component molar density. If this is done, then the equation which results is

---

*The Implicit Pressure-Explicit Saturation (IMPES) procedure is a common reservoir simulation technique in which the pressure solution is solved implicitly over the entire reservoir, followed by a point-by-point explicit saturation solution.

Table 2.1 - Iteration Variables and Equati

PT variables *	P_j^n	T_j^n	$(S_g)_j^n$	$(q_T)_j^n$	TOTAL
# of variables	$N-N_G-1$	$N-1$	N_G	2	2N
SX variables	$(S_w)_j^n$	$(S_o)_j^n$	$(x_i)_j^n$		TOTAL
# of variables	N	0	$(C-1)N$		CN
PT equations	(2.19)	(2.22)	(2.23)		TOTAL
# of equations	N	N	0		2N
SX equations	(2.27)	(2.28)			TOTAL
# of equations	$(C-1)N$	N			CN

*It is assumed that there is vapour at the injection boundary, and no vapour at the production boundary.

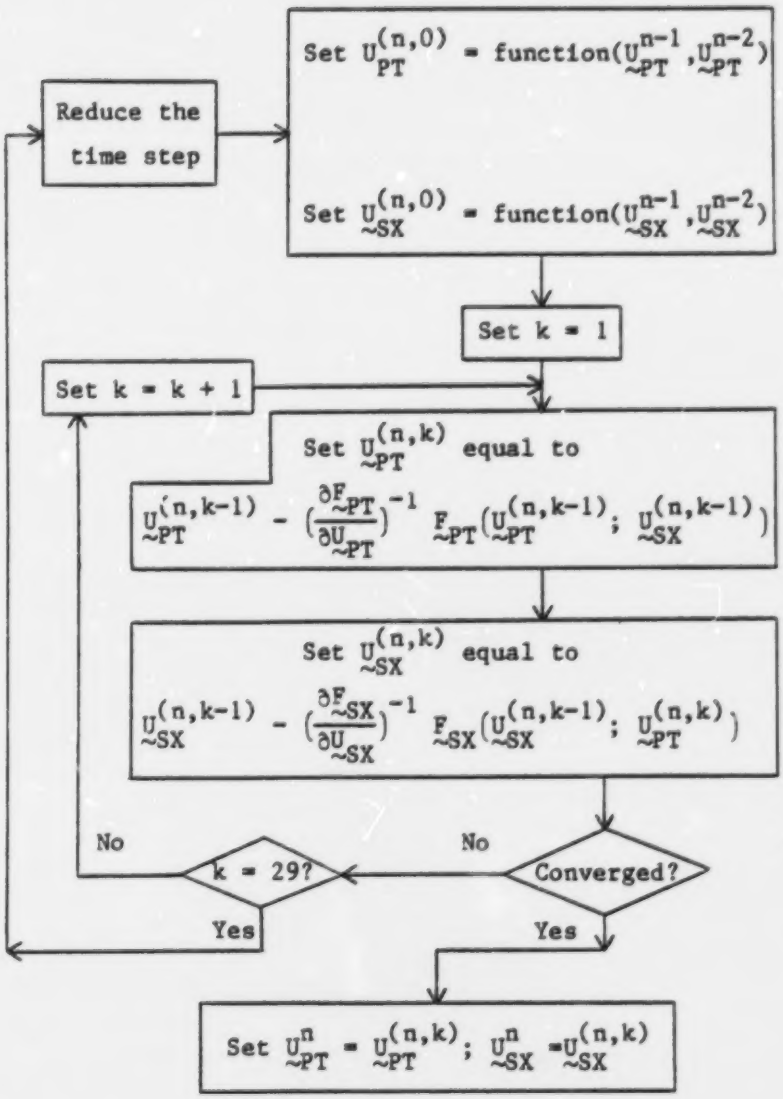
Reduce the time step
Set $U_{PT}^{(n,0)}$ = function($U_{\sim PT}^{n-1}$, $U_{\sim PT}^{n-2}$)
Set $U_{SX}^{(n,0)}$ = function($U_{\sim SX}^{n-1}$, $U_{\sim SX}^{n-2}$)
Set k = 1
Set k = k + 1
Set $U_{\sim PT}^{(n,k)}$ equal to
$U_{\sim PT}^{(n,k-1)} - (\frac{\partial F_{\sim PT}}{\partial U_{\sim PT}})^{-1} F_{\sim PT}(U_{\sim PT}^{(n,k-1)}; U_{\sim SX}^{(n,k-1)})$
Set $U_{\sim SX}^{(n,k)}$ equal to
$U_{\sim SX}^{(n,k-1)} - (\frac{\partial F_{\sim SX}}{\partial U_{\sim SX}})^{-1} F_{\sim SX}(U_{\sim SX}^{(n,k-1)}; U_{\sim PT}^{(n,k)})$
No
k = 29?
Yes
No
Converged?
Yes
Set $U_{\sim PT}^{n} = U_{\sim PT}^{(n,k)}$; $U_{\sim SX}^{n} = U_{\sim SX}^{(n,k)}$

Figure 2.1. The proposed two-level method.

$$\frac{1}{\delta t}\left[\sum_{p,i}\frac{(\phi S_p\rho_p w_i)_j^n}{(\rho_{p,i})_j^n}-\sum_{p,i}\frac{(\phi S_p\rho_p w_i)_j^{n-1}}{(\rho_{p,i})_j^n}\right]$$

$$=\frac{1}{X_{j+\frac{1}{2}}-X_{j-\frac{1}{2}}}\sum_{p,i}\frac{\Delta_X(T_p w_i\Delta_X P)_j^n}{(\rho_{p,i})_j^n}+\sum_{p,i}\sigma_p\frac{(M_i)_j^n}{(\rho_{p,i})_j^n} \qquad (2.17)$$

The first term in equation (2.17) can be simplified by the assumption that

$$\sum_i\frac{w_i}{\rho_{p,i}}=\frac{1}{\rho_p} \qquad (2.18)$$

The last term in equation (2.17) can be simplified since we are assuming that no component is present in more than one liquid phase. The result of these two simplifications is equation (2.19), an overall volume balance.

$$\frac{1}{\delta t}\left[\phi_j^n-\sum_{p,i}\frac{(\phi S_p\rho_i w_i)_j^{n-1}}{(\rho_{p,i})_j^n}\right]$$

$$=\frac{1}{X_{j+\frac{1}{2}}-X_{j-\frac{1}{2}}}\sum_{p,i}\frac{\Delta_X(T_p w_i\Delta_X P)_j^n}{(\rho_{p,i})_j^n}$$

$$+\sum_i(M_i)_j^n\left(\frac{1}{\rho_{\ell,i}}-\frac{1}{\rho_{g,i}}\right)_j^n \qquad (2.19)$$

In a similar manner, it is possible to eliminate the unknown saturation terms from the enthalpy balance. This can be done by multiplying each component-phase mole balance by the component molar enthalpy, by adding all the resulting equations together,

$$\frac{1}{\delta t}\left[\sum_{p,i}(\phi S_p\rho_p w_i h_{p,i})_j^n - \sum_{p,i}(\phi S_p\rho_p w_i)_j^{n-1}(h_{p,i})_j^n\right]$$
$$= \frac{1}{X_{j+\frac{1}{2}}-X_{j-\frac{1}{2}}}\sum_{p,i}(h_{p,i})_j^n\Delta_X(T_p w_i\Delta_X P)_j^n$$

$$+\sum_{p,i}\sigma_p(M_i)_j^n(h_{p,i})_j^n \qquad (2.20)$$

and by subtracting the resulting equation (2.20) from the enthalpy balance (2.2), as is explained in the next paragraph.

The first term in equation (2.20) can be simplified by the assumption that

$$\sum_i w_i h_{p,i} = h_p \qquad (2.21)$$

The last term in equation (2.20) can be simplified because we are assuming that no component is present in more than one liquid phase. Therefore, the result of subtracting equation (2.20) from the enthalpy balance (2.2) is

$$\frac{1}{\delta t}\{[1-\phi)\rho_r h_r]_j^n$$

$$+\sum_p(\phi S_p\rho_p)_j^{n-1}\left[\sum_i(w_i)_j^{n-1}(h_{p,i})_j^n - (h_p)_j^{n-1}\right]\}$$

$$= \frac{1}{X_{j+\frac{1}{2}}-X_{j-\frac{1}{2}}} \Delta_X\Big(\sum_p T_p h_p \Delta_X P\Big)_j^n$$

$$- \frac{1}{X_{j+\frac{1}{2}}-X_{j-\frac{1}{2}}} \sum_{p,i} (h_{p,i})_j^n \Delta_X(T_p w_i \Delta_X P)_j^n$$

$$+ \frac{1}{X_{j+\frac{1}{2}}-X_{j-\frac{1}{2}}} \Delta_X(T_c \Delta_X T)_j^n - \sum_i (M_i)_j^n (h_{\ell,i}-h_{g,i})_j^n$$

$$- (q_L)_j^n \ , \quad j=1,\ldots,N \qquad (2.22)$$

By means of the above manipulations, the influence of the unknown saturations and compositions on the terms of equations (2.19) and (2.22) has been reduced significantly. Therefore, if reasonable guesses are made for the oil and water saturations and for the oil compositions, then the sets of equations (2.19) and (2.22) can be solved simultaneously to obtain good approximations for the temperatures, pressures, and vapour saturations.

The condensation rates can be eliminated from equations (2.19) and (2.22) by substituting a rearranged version of the vapour phase mole balances (2.1):

$$(M_i)_j^n = \frac{1}{X_{j+\frac{1}{2}}-X_{j-\frac{1}{2}}} \Delta_X(T_g y_i \Delta_X P)_j^n - \frac{1}{\delta t}(\phi S_g \rho_g y_i)_j^n$$

$$+ \frac{1}{\delta t}(\phi S_g \rho_g y_i)_j^{n-1} \ , \ j=1,\ldots,N \ , \ i=1,\ldots,C+1 \qquad (2.23)$$

One noteworthy property of the PT variables is that once the PT equations are solved, a new value is provided for the vapour saturations $(S_g)_j$, but not for the liquid-phase saturations $(S_w)_j$ and $(S_o)_j$. This causes the sum of the phase saturations to be different from 1. One solution to this problem is to change the liquid-phase saturations using the equations

$$(\Delta S_g)_j^{(n,k)} = (S_g)_j^{(n,k)} - (S_g)_j^{(n,k-1)}$$

$$(S_w)_j^{(n,k-\frac{1}{2})} = (S_w)_j^{(n,k-1)} - (f_{Dw})_j^{(n,k)}(\Delta S_g)_j^{(n,k)}$$

$$(S_o)_j^{(n,k-\frac{1}{2})} = (S_o)_j^{(n,k-1)} - (1-f_{Dw})_j^{(n,k)}(\Delta S_g)_j^{(n,k)}$$

where f_{Dw} is calculated via a formula designed to improve the rate of convergence of the iteration method. The formula for f_{Dw} which is used in the simulator is

$$(f_{Dw})_j^{(n,k)} = \frac{(S_w)_j^{(n,k-1)} - (S_w)_j^{(n,k-2)}}{[(S_w)_j^{(n,k,-1)} - (S_w)_j^{(n,k-2)}] + [(S_o)_j^{(n,k-1)} + (S_o)_j^{(n,k-2)}]} \quad (2.24)$$

However, if formula (2.24) yields a number outside the interval $[0,1]$, then $(f_{Dw})_j$ is set to either 0 or 1 (whichever is closer). Furthermore, if the denominator of the right-hand-side of (2.24) is close to 0, then $(f_{Dw})_j$ is left at its previous iterate value.

Alternatives to equation (2.24) were not extensively investigated. Hence, it may be possible to devise a more effective estimator of phase saturation

changes. However, limited experimentation indicates that if f_{Dw} is calculated using formula (2.24), the two-level procedure converges more than 1½ times as quickly as it does when f_{DW} is set to a constant such as 0.5.

2.4 The SX Equations

Implicit equations for the liquid saturations and the oil-phase compositions are obtained directly from the liquid-phase component mole balances (2.1) and from the assumption that no component is present in more than one liquid phase. Since the PT equations include N volume balances (2.19), the complete set of liquid-phase component mole balances is overdetermined. This redundancy can be eliminated by replacing the mole balances for water and for one of the oil components (e.g., the heaviest oil) with a linear combination of the two mole balances. This linear combination is derived by multiplying the mole balances for component C and for water by $(\bar{\lambda}_{C+1})_j^n$ and $(\bar{\lambda}_C)_j^n$ respectively, where

$$(\bar{\lambda}_{C+1})_j^n = \begin{cases} (T_w)_{1+\frac{1}{2}}^n (P_1^n - P_2^n) + (J_w)_1^n (q_T \rho_w)_1^n & , j=1 \\ \dfrac{(\tau_w)_{j+\frac{1}{2}}^n}{X_{j+1}-X_j} + \dfrac{(\tau_w)_{j-\frac{1}{2}}^n}{X_j - X_{j-1}} & , j=2,3,\ldots,N \end{cases} \tag{2.25}$$

and

$$(\bar{\lambda}_C)_j^n = \begin{cases} (T_o)_{1\frac{1}{2}}^n (P_1^n - P_2^n) + (J_o)_1^n (q_T \rho_o x_C)^n \ , & j=1 \\ (T_o x_C)_{j+\frac{1}{2}}^n + (T_o x_C)_{j-\frac{1}{2}}^n \ , & j=2,3,\ldots,N \end{cases} \tag{2.26}$$

and by then subtracting one balance from the other. Therefore, the SX equations are

$$\frac{1}{\delta t}\left[(\phi S_\ell \rho_\ell x_i)_j^n - (\phi S_\ell \rho_\ell x_i)_j^{n-1}\right] = \frac{1}{X_{j+\frac{1}{2}} - X_{j-\frac{1}{2}}} \Delta_X (T_\ell x_i \Delta_X P)_j^n + (M_i)_j^n \ ,$$

$$j=1,\ldots,N \ , \ i=1,\ldots,C-1 \tag{2.27}$$

and

$$\begin{aligned} &\frac{1}{\delta t}(\bar{\lambda}_{C+1})_j^n \left[(\phi S_o \rho_o x_C)_j^n - (\phi S_o \rho_o x_C)_j^{n-1}\right] \\ &- \frac{1}{\delta t}(\bar{\lambda}_C)_j^n \left[(\phi S_w \rho_w)_j^n - (\phi S_w \rho_w)_j^{n-1}\right] \\ &= \frac{1}{X_{j+\frac{1}{2}} - X_{j-\frac{1}{2}}} \left[(\bar{\lambda}_{C+1})_j^n \Delta_X (T_o x_C \Delta_X P)_j^n \right. \\ &\left. - (\bar{\lambda}_C)_j^n \Delta_X (T_w \Delta_X P)_j^n\right] \\ &+ (\bar{\lambda}_{C+1} M_C)_j^n - (\bar{\lambda}_C M_{C+1})_j^n \ , \ j=1,\ldots,N \end{aligned} \tag{2.28}$$

Although it would have been feasible to simply throw out one of the mole balance equations, rather than to combine the balances to get equations (2.27) and (2.28), we chose to opt for the more complex treatment with the expectation that the coupling between the PT and SX equations could be reduced. By means of this linear combination, the major terms of the equations that cause coupling are reduced significantly. This modification was found to improve the efficiency of the algorithm considerably.

Although the pressures and temperatures are counted as PT variables, it does not follow that they remain constant during the SX-level of the two-level iteration procedure. The pressures and temperatures in the region without a vapour phase do remain constant. However, the pressures and temperatures in the region containing a vapour phase are coupled with the oil-phase mole fractions. Therefore, it is reasonable to assume that the performance of the two-level iteration procedure is improved if one ensures that when the oil-phase mole fractions are adjusted during the SX level, then either the pressures or the temperatures (or both) in the region containing a vapour phase should also be adjusted so that vapour-liquid equilibrium is maintained. As part of our program to streamline the simulator, an investigation was made to determine whether it is better to keep the temperatures constant and adjust the pressures, or to keep the pressures constant and adjust the temperatures. The constant-temperature-adjusted-pressure alternative has the advantage that it is considerably easier to calculate the pressures from the temperature (and oil-phase mole fractions) using the vapour-pressure equations in the appendix, than it is to solve these equations implicitly for the temperatures, if the pressures (and oil-phase mole fractions) are given. On the other hand, the constant-pressure-adjusted-temperature alternative has the advantage that the

two-level iteration procedure requires considerably fewer iterations per time step.

When the simulator was run with the constant-temperature-adjusted-pressure method on the test problem with 11 grid blocks, the simulated steam front advanced through the first 6 grid blocks in 124 time steps, which required a total of 1470 iterations or 11.9 iterations per time step. When the simulation was performed on the same input data, using the constant-pressure-adjusted-temperature method together with the modification discussed in the next paragraph, the simulated steam front advanced through the same 6 grid blocks in 99 time steps, which required a total of 845 iterations or 8.5 iterations per time step for larger time steps. Since at least half of this improvement may be attributed to the constant-pressure-adjusted-temperature method, we conclude that the speed advantage of this method more than compensates for its increased complexity. Since this comparison was made, further improvements to the constant-pressure-adjusted-temperature method were made. As a result, when the simulation was performed on the same input data as was used for the other two simulations, the simulated steam front advanced through the same 6 grid blocks in 94 time steps, which required a total of 561 iterations, or 6.0 iterations per time step for yet larger time steps.

One special case required a further modification of the SX-level. During some time steps, the water saturation drops rapidly towards the connate water saturation. Because of the nature of the water-permeability and oil-permeability formulae, the Jacobian sometimes varies significantly from iteration to iteration during the calculations for these time steps. These variations retard the convergence of the iteration. Therefore, the simulator was modified so that whenever a water saturation is above the connate value in

one iteration, and below the connate value in the next iteration, (or vice versa), then the two iterate values are averaged, i.e.

$$S_{w,j}^{(n,k)} \leftarrow \tfrac{1}{2}(S_{w,j}^{(n,k,\ \text{tentative})} + S_{w,j}^{(n,k-1)}) \tag{2.29}$$

$$S_{o,j}^{(n,k)} \leftarrow \tfrac{1}{2}(S_{o,j}^{(n,k,\ \text{tentative})} + S_{o,j}^{(n,k-1)}) \tag{2.30}$$

This modification results in a significant reduction in the number of iterations required during the relatively small number of time steps in which larger changes in water saturation occur.

2.5 Results and Discussion

Coats[1] examines two problems, which are intended to illustrate the superiority of a highly implicit model over a particular sequential model. Since the second of these problems includes a distillable oil component, we selected a modified version of this problem as a test of the present iterative procedure. The modifications include:

(1) a one-dimensional grid with 10 blocks totalling 68.2 m instead of a 5 x 3 x 2 grid totalling 195 ft in the x-direction,

(2) a constant-pressure boundary condition at both the injection and production wells,

(3) zero capillary pressures,

(4) temperature-invariant permeabilities,

(5) different formulae for the heat capacities, the latent heats of vaporization, the K_i ($K_i = y_i/x_i$), the rock density, and the vapour-phase density and viscosity,

(6) a lower quality for the injected steam, and

(7) no heat loss in the transverse direction.

Figure 2.2 contains a plot of the temperature and vapour saturation as a function of position, after approximately 0.6 pore volumes (cold-water-equivalent) of steam and water have been injected, i.e. after approximately 531 days of simulated time. These results are qualitatively consistent with those reported by Coats.

One of the disadvantages of previous sequential simulators is a failure to preserve material and enthalpy balances. To the contrary, since our simulator uses an iterative method to solve a highly implicit set of equations, it is capable of preserving material and enthalpy balances. Indeed, after the 531 day simulation described above, all balance errors were smaller than 10^{-3}%.

One of the advantages of the proposed 2-level method is the savings in computation time which result from solving two smaller systems of linear equations instead of one large system. However, since the solution of large systems of equations is not the only calculation which requires a large amount of computer time, the potential savings in computer time have been investigated in greater detail. Simulations were carried out for a 10-block grid and for a 5-block grid, so that the computation time required for different parts of the calculation could be evaluated. The calculation times were converted to seconds per time step, assuming 7 iterations per time step, and were used to construct estimates, based on the details of the computer program, of how the computation times of the different calculations scale with the number of oil-phase components and with the number of grid blocks. Estimates were also made of how the computation times of the different calculations would scale if Coats' highly implicit method were used, assuming that 4 iterations per time

step are required[1], and assuming that the calculations are carried out the same way. (Clearly, the computation times can be reduced if the solution of the linear equations is programmed in assembler language, if inaccurate but simple formulae for the elements of the Jacobian matrix can be used without decreasing the rate of convergence of the iterative method, or if more table look-ups are used for the calculation of material properties.) Table 2.2 lists the formulae for estimating the computation time requirement of the various phases of the calculation. Table 2.3 contains estimates, calculated using the formulae of table 2.2, of the total computation time requirement of the two methods, for problems of several representative sizes.

For one-dimensional problems, the calculation of the Jacobian matrix requires more computation time than any other phase of the simulation. However, for two-dimensional simulations, as the number of grid blocks increases, and as the number of oil-phase components increases, the computation time required to solve the systems of linear equations soon dominates the computation time required for all the other calculations. Therefore, the speed of the two-level method in solving the systems of linear equations more than compensates for the extra iterations per time step that are required.

The one problem with this comparison is with the calculation of the Jacobian(s). Coats has shown[1] how a simple, but adequate approximation to the Jacobian can be derived for the highly implicit method. On the other hand, the current implementation of the two-level method includes formulae for the Jacobian, which are long, complicated, computationally expensive, and difficult to program. (The two-level procedure, as a whole, is rather difficult to program.) It remains to be seen how much these formulae can be simplified.

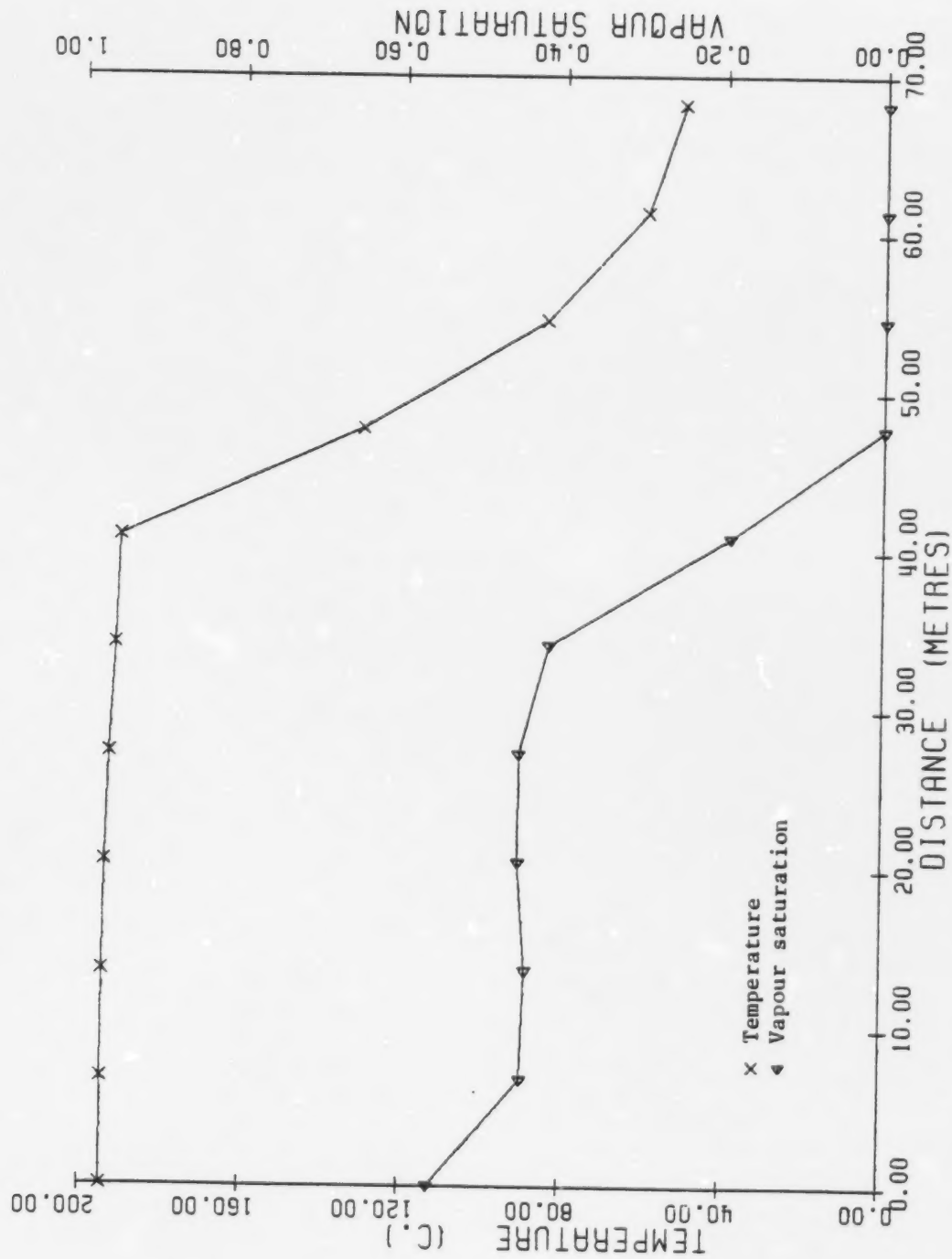

Figure 2.2 - Profiles of temperature and vapour saturation after 0.6 pore volumes were injected (45,900,000 sec., 10 grid blocks)

TABLE 2.2 - FORMULAE TO ESTIMATE COMPUTATION TIME

computation time : seconds per time step
grid : N x M, N > M

C = number of components in the oil phase
$B = \begin{cases} N + M & \text{if } M > 1 \\ 1 & \text{if } M = 1 \end{cases}$
D_4 : savings obtained by using D4 ordering

2-Level Procedure (7 iterations per time step)

OPERATION	FORMULA
SET UP JACOBIAN	
Gas Sat.-Pressure-Temp.	$0.0195\ B + 0.0091\ MN$
Saturation-Composition	$[0.0126\ B + 0.0124\ MN] \times [C(0.33 + 0.088(C-3))]$
SOLVE LINEAR EQUATIONS	
Gas Sat.-Pressure-Temp.	$0.00040\ M(N+1)(M+1)^2 D_4$
Saturation-Composition	$0.000047\ MN\ C^3\ (M+1)^2\ D_4$
EVALUATE MATERIAL PROPERTIES	$[0.0230\ B + 0.0072\ MN] \times [1 + 0.35(C-3)]$
OTHERS	$[40.0 + 10.8\ B + 5.4\ MN] \times 0.001 \times [1 + 0.3(C-3)]$

1-Level Procedure (4 iterations per time step)

OPERATION	FORMULA
SET UP JACOBIAN	
Gas Sat.-Pressure-Temp. part	$[0.0111\ B + 0.0052\ MN] \times [1.7 + 0.15(C-3)]$
Saturation-Composition part	$+ [0.0072\ B + 0.0071\ MN] \times [C(0.49 + 0.088(C-3))]$
SOLVE LINEAR EQUATIONS	$0.000027\ MN\ (C+2)^3\ (M+1)^2\ D_4$
EVALUATE MATERIAL PROPERTIES	$[0.0079\ B + 0.0025\ MN] \times [1 + 0.35(C-3)]$
OTHERS	$[22.9 + 6.2\ B + 3.1\ MN] \times 0.001 \times [1 + 0.3(C-3)]$

TABLE 2.3 - COMPARISON OF ESTIMATED COMPUTATION TIME FOR THE 2-LEVEL AND 1-LEVEL PROCEDURES

M	N	C	D_4	COMPUTATION TIME (SECONDS/TIME STEP)		RATIO
				PRESENT METHOD	1-LEVEL METHOD	$\frac{\text{1-LEVEL}}{\text{2-LEVEL}}$
1	6	3	1.000	0.35	0.30	0.85
1	12	3	1.000	0.59	0.53	0.89
1	12	2	1.000	0.40	0.34	0.86
4	10	2	1.000	2.4	2.9	1.2
4	10	4	1.000	6.5	8.0	1.2
4	10	6	1.000	15.6	17.2	1.1
8	8	2	0.583	4.6	6.9	1.5
12	12	2	0.437	12.8	21.7	1.7

2.6 Conclusions

An iterative method has been developed for solving the first-order implicit finite-difference approximation to the equations governing steam injection into a heavy oil reservoir. This method combines the stability and material and enthalpy balance accuracy of Coats' highly implicit method, with the smaller systems of linear equations characteristic of IMPES and IMPES-like methods. For 2-dimensional and 3-dimensional simulations, the computation time required to solve the systems of linear equations dominates the computation time required for the simulation. Therefore, as the number of grid blocks increases, the advantage of solving smaller systems of linear equations becomes increasingly significant. However, this advantage can be fully realized by the proposed iterative method only if a more computationally efficient approximation for the Jacobian is implemented.

3. THE NUMERICAL SIMULATION WITH FRONT-TRACKING

3.1 The Moving Grid Point

The basic idea of our front-tracking method is to modify a standard (one-dimensional) finite-difference "grid" by adding one moving grid point whose location is at the interface between the region containing steam and the region which does not contain steam. The location of the interface and, hence, of the moving grid point, is a function of time and is an unknown, which must be solved for simultaneously with the other unknowns at each time step. In this respect, our method differs from most published methods of handling moving boundary conditions (e.g. Fong and Skidmore[10]), which estimate the velocity of the moving boundary based on an explicit formulation, and then

perform the other calculations, without updating or otherwise correcting the original estimate of the moving boundary's velocity.

Since the saturations are discontinuous at the interface between the region with steam and the region without steam, the phase flow rates are also discontinuous, with significant condensation occurring at the front. Therefore, it is necessary to derive matching conditions which relate the flow rates and saturations on one side of the interface to the flow rates and saturations on the other side of the interface. Since the matching conditions must be solved simultaneously with the other finite-difference equations, it is necessary to check that the resulting system of equations does not contain more equations than unknowns.

Because of the discontinuities in the saturations at the front, it is desirable to arrange the grid blocks so that the moving grid point is at the border between two grid blocks. (We arrived at this conclusion after several unsuccessful front-tracking formulations.) Therefore, the m-th grid block was eliminated (where m denotes the subscript which refers to the moving grid point, when all the grid points are numbered in standard order (i.e. $X_1<X_2<\ldots X_m<\ldots X_N$)), and the (m-1) and (m+1) grid blocks were extended to X_m. This device places the location of the moving grid point ($X=X_m$) at the border between two grid blocks.

Since the only differences (e.g. different sizes of grid blocks) between the modified grid and the standard grid occur in the vicinity of the moving grid point, the finite-difference equations for the modified grid with front-tracking are the same as the respective finite-difference equations for the standard grid everywhere, except in the vicinity of the moving grid point, (i.e. at j=m-1, m, and m+1).

In the next section, matching conditions which relate the flow rates and saturations on the two sides of the interface are derived. Section 3.3 describes finite-difference approximations for the matching conditions, and the modified finite-difference approximations to the grid balance equations for the (m-1) and (m+1) grid blocks. Section 3.4 shows how the two-level iterative method was modified to accommodate these changes. Finally, section 3.5 describes the performance of the modified finite-difference method.

3.2 Matching Conditions

3.2.1 An Illustration of Matching

Matching conditions for the interface between the region with vapour and the region without vapour can be derived via material and enthalpy balances on a small stationary control volume which contains the interface. Before this is done, however, it is useful to construct the matching condition for the simpler problem of axial heat conduction through two bars of different thermal conductivity attached end-to-end at $X=X_B$.

Due to the discontinuity in material properties at X_B, the thermal conductivity of the composite bar may be represented by

$$k(x) = \begin{cases} k^- , & X < X_B \\ k^+ , & X > X_B \end{cases}$$

Now suppose that the temperature of the bar is a function of X alone. In order to derive a matching condition for such heat transfer problems, we construct a small control volume around $X=X_B$ as shown in figure 3.1.

The heat balance over the control volume can be expressed as

$$\begin{bmatrix}\text{change in enthalpy}\\ \text{within the control}\\ \text{volume}\end{bmatrix} = \begin{bmatrix}\text{amount of enthalpy}\\ \text{flowing through}\\ \text{left boundary}\end{bmatrix} - \begin{bmatrix}\text{amount of enthalpy}\\ \text{flowing through}\\ \text{right boundary}\end{bmatrix} \qquad (3.1)$$

A mathematical formulation of equation (3.1) is

$$C_p \frac{\partial T}{\partial t} A\Delta X\delta t + o(\delta t\Delta X) =$$

$$A\delta t \left[-k\frac{\partial T}{\partial X}\right]_{X_B-\Delta X/2} + A\delta t \left[k\frac{\partial T}{\partial X}\right]_{X_B+\Delta X/2} + o(\delta t) \qquad (3.2)$$

where A = cross-sectional area of the bar,

T = temperature,

ΔX = width of the control volume,

C_p = heat capacity of the bar per unit volume,

δt = length of time over which the balance is calculated,

and the "o" terms * signify the magnitude of the errors made in the balance for finite magnitude δt and ΔX. Therefore, the balance over the control volume can be rewritten as

$$(C_p\frac{\partial T}{\partial t})(A\Delta X)\delta t = (-k\frac{\partial T}{\partial X}\Big|^{-})A\delta t + (k\frac{\partial T}{\partial X}\Big|^{+})A\delta t + o(\delta t) + o(\Delta X)$$

*See the note on the little "o" notation in the Nomenclature section.

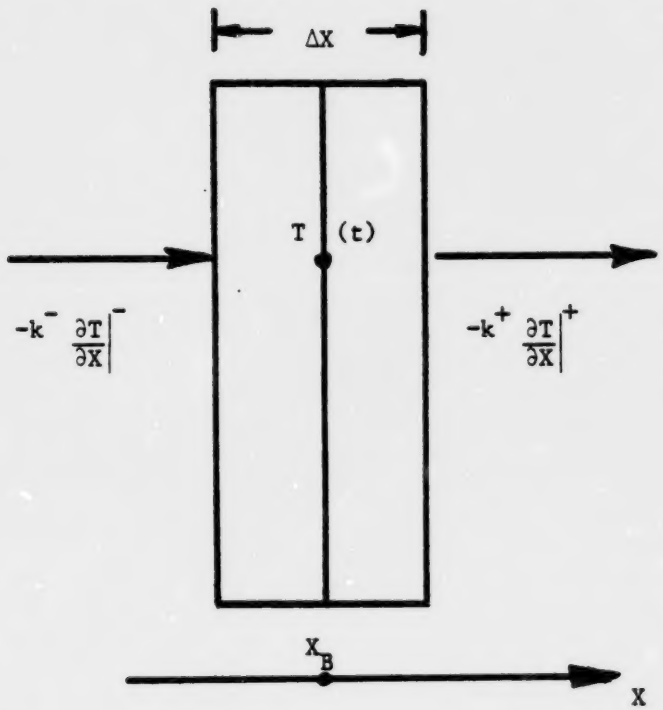

Figure 3.1 - Control Volume for Linear Conduction in Simple Bimaterial

Since A and δt are non-zero (although δt is small), this equation can be divided by $A\delta t$ with the result that

$$(C_p\frac{\partial T}{\partial t})\Delta X = k^+\frac{\partial T}{\partial X}\Big|^+ - k^-\frac{\partial T}{\partial X}\Big|^- + o(1) + o(\frac{\Delta X}{\delta t}) \qquad (3.3)$$

If we assume the continuum hypothesis (i.e. neglecting quantum effects), then since the interface has zero thickness, it is possible to derive equation (3.3) for control volumes of arbitrarily small, but positive ΔX. Therefore, the terms $(C_p\frac{\partial T}{\partial t})\Delta X$, $o(1)$ and $o(\frac{\Delta X}{\delta t})$ may be neglected, in the lim $\Delta X \to 0$, $\delta t \to 0$, with the result that

$$k^+\frac{\partial T}{\partial X}\Big|^+ = k^-\frac{\partial T}{\partial X}\Big|^- \qquad (3.4)$$

This is the matching condition known to be appropriate for the two-material heat conduction problem.

3.2.2 The Moving Interface Problem

The problem of deriving matching conditions for the steam injection problem is more complicated than the preceding illustrative example. However, the principle is the same. Consider the section of a reservoir shown in figure 3.2 into which steam is being injected. The variables of interest are assumed to be a function of X alone. Suppose that region I contains vapour, region II contains no vapour, and that the steam front may be modelled as a sharp interface at $X=X_B$ between the two regions. The problem here is to derive the matching conditions valid at $X=X_B$.

The phase saturations can be assumed to be differentiable functions of X,

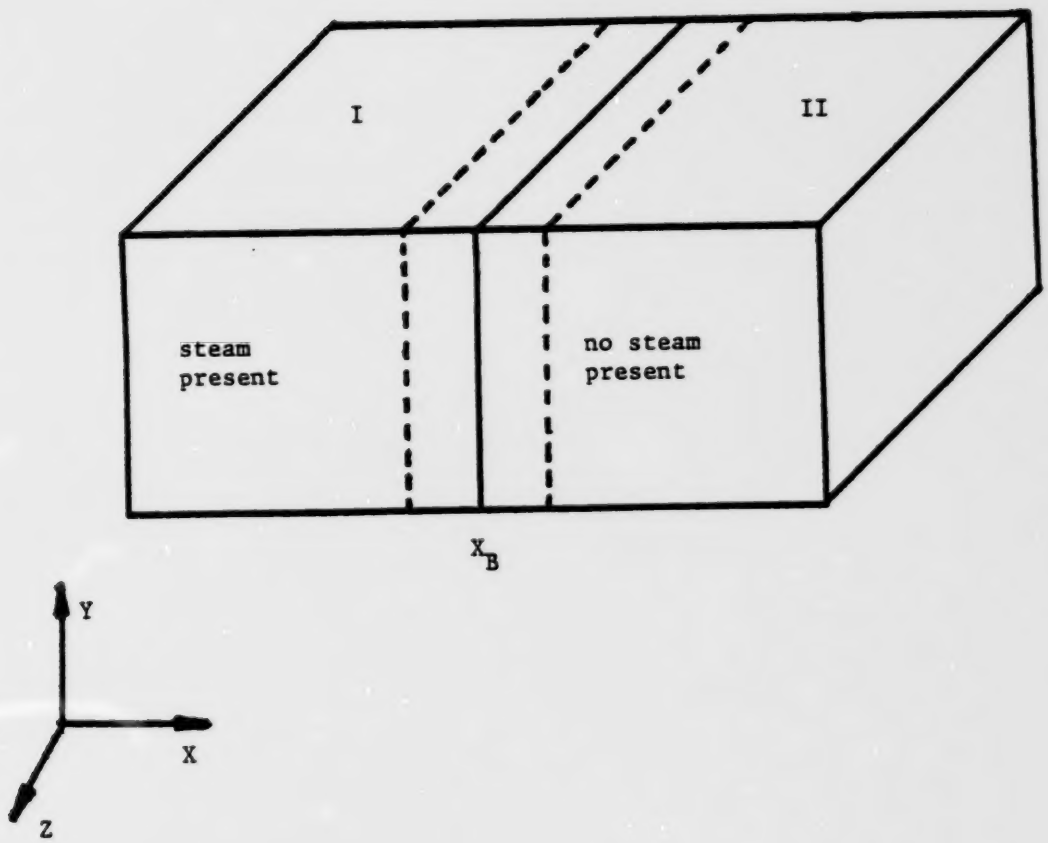

Figure 3.2 - Steam Injection

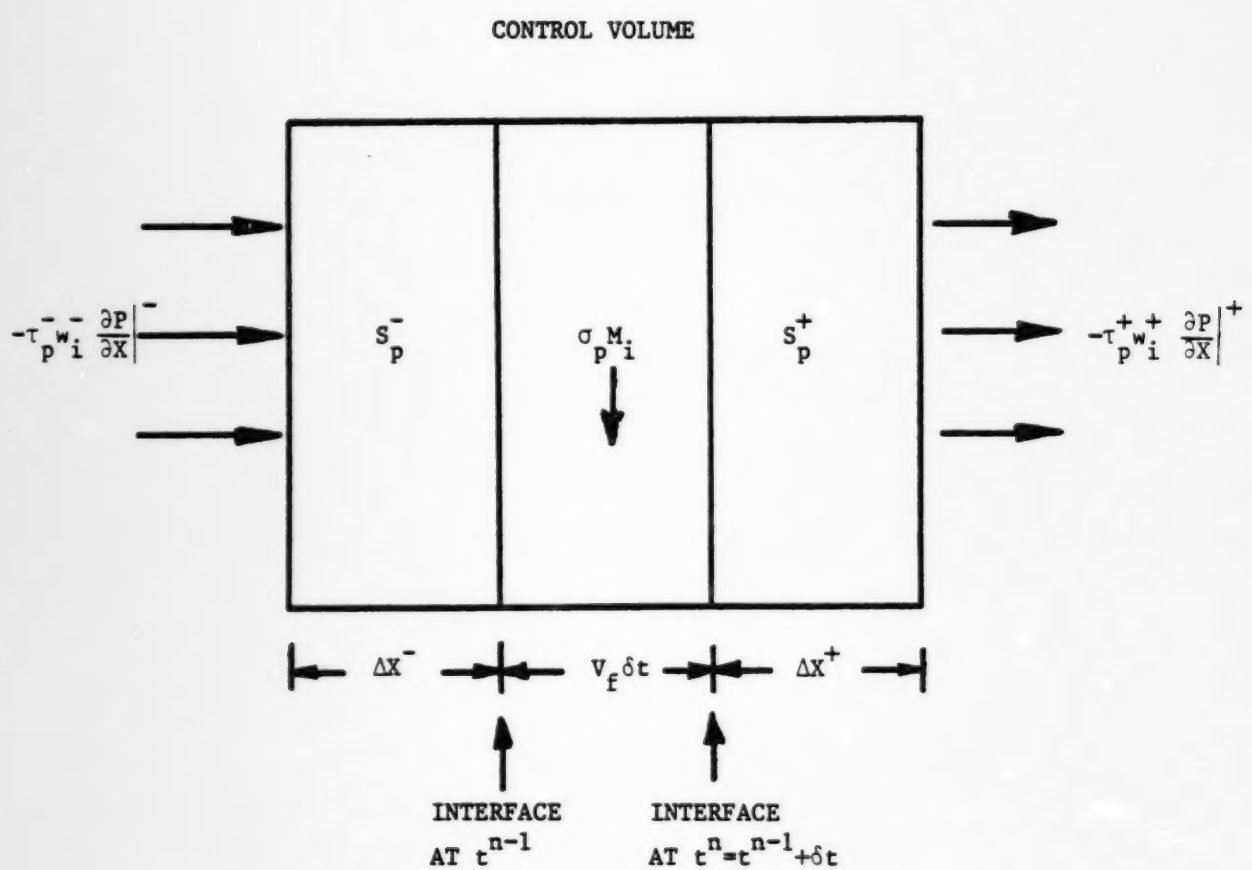

Figure 3.3 Control Volume for Steam Injection Problem

Table 3.1 Material balance on species i in phase p

$$(\phi^- S_p^- \rho_p^- w_i^-)^n A(\Delta X^- + V_f \delta t) + (\phi^+ S_p^+ \rho_p^+ w_i^+)^n A \Delta X^+$$

amount of component i in phase p at t^n

$$- (\phi^- S_p^- \rho_p^- w_i^-)^{n-1} A(\Delta X^-) - (\phi^+ S_p^+ \rho_p^+ w_i^+)^{n-1} A(\Delta X^+ + V_f \delta t)$$

amount of component i in phase p at t^{n-1}

$$+ o(\Delta X^- + V_f \delta t + \Delta X^+) *$$

order of the error

$$= - \left(\tau_p^- w_i^- \frac{\partial P}{\partial X}\bigg|^-\right)^n A \delta t + \left(\tau_p^+ w_i^+ \frac{\partial P}{\partial X}\bigg|^+\right)^n A \delta t$$

advection into the control volume — advection out of the control volume

$$+ \sigma_p M_i^n A(\Delta X^- + V_f \delta t + \Delta X^+) \delta t$$

gain by the phase due to condensation

$$+ o(\Delta X^- + V_f \delta t + \Delta X^+) + o(\delta t)$$

order of the error (3.5)

*See the note on the little "o" notation in the Nomenclature section.

except at $X=X_B$, where they are discontinuous. In addition, it is reasonable to assume that the pressure, temperature, and compositions of the phases are continuous and continuously differentiable functions of X, except at $X=X_B$, where they are continuous, but their derivatives may be discontinuous.

For the purpose of deriving matching conditions for this moving interface problem, a small stationary control volume is constructed around the interface at $X=X_B$, large enough that the interface is always inside the control volume during a period of duration δt, as in figure 3.3. The balance for species i consists basically of an accounting of all flows of the species in and out of the control volume during the time interval δt. The net flow into the control volume is accounted for as a "change" in the contents of the control volume. Using the nomenclature defined in the Nomenclature section and in figure 3.3, we have constructed the material balance for species i in phase p, which is given in table 3.1 as equation (3.5). After equation (3.5) is divided by $A\delta t$, and the time-level differences on the left side of the equation are replaced by partial derivatives with respect to t, plus $o(\delta t)$ terms, the equation which results is

$$\left(\frac{\partial(\phi^- S_p^- \rho_p^- w_i^-)}{\partial t}\right)\Delta X^- + \left(\frac{\partial(\phi^+ S_p^+ \rho_p^+ w_i^+)}{\partial t}\right)(\Delta X^+ + V_f \delta t)$$

$$+ \left[(\phi^- S_p^- \rho_p^- w_i^-) - (\phi^+ S_p^+ \rho_p^+ w_i^+)\right] V_f = \left(\tau_p^+ w_i^+ \frac{\partial P}{\partial X}\bigg|^+\right)$$

$$-\left(\tau_p^- w_i^- \frac{\partial P}{\partial X}\bigg|^-\right) + \sigma_p M_i (\Delta X^- + V_f \delta t + \Delta X^+) + o\left(\frac{\Delta X^-}{\delta t} + V_f + \frac{\Delta X^+}{\delta t}\right) + o(1) \qquad (3.6)$$

Finally, we can take the limit of this equation as ΔX^- and ΔX^+ go to zero, and subsequently as $\delta t \to 0$. The condensation term, however, requires some special consideration since, at the steam front, intense condensation (or evaporation) will be taking place. This condensation may be represented as a point source at $X=X_B$. Hence, even in the limit $\Delta X^+ \to 0$, $\Delta X^- \to 0$, and $\delta t \to 0$, the condensation term will remain finite. Thus, the matching condition becomes

$$(\phi^- S_p^- \rho_p^- w_i^- - \phi^+ S_p^+ \rho_p^+ w_i^+) V_f = \tau_p^+ w_i^+ \left.\frac{\partial P}{\partial X}\right|^+ - \tau_p^- w_i^- \left.\frac{\partial P}{\partial X}\right|^- + \sigma_p \bar{M}_i \quad , \; i=1,\ldots,C+1 \qquad (3.7)$$

where $\bar{M}_i$ is the finite magnitude, "point source" condensation term.

The derivation of the enthalpy matching condition parallels the derivation of the material matching conditions. A small stationary control volume is constructed around $X=X_B$, large enough that the interface is always inside the control volume during the period of duration δt, as in figure 3.3. An enthalpy balance is performed on this control volume.

After considerable manipulation the enthalpy matching condition becomes:

$$\begin{aligned}(\phi^- \textstyle\sum_p S_p^- \rho_p^- h_p^- - \phi^+ \sum_p S_p^+ \rho_p^+ h_p^+) V_f + [(1-\phi^-)\rho_r^- h_r^- \\ -(1-\phi^+)\rho_r^+ h_r^+] V_f = \textstyle\sum_p \tau_p^+ h_p^+ \left.\frac{\partial P}{\partial X}\right|^+ - \sum_p \tau_p^- h_p^- \left.\frac{\partial P}{\partial X}\right|^- \\ + k_c^+ \left.\frac{\partial T}{\partial X}\right|^+ - k_c^- \left.\frac{\partial T}{\partial X}\right|^- \end{aligned} \qquad (3.8)$$

where $\sum_p$ denotes summation over all phases.

The matching conditions yield new constraints which must be used to solve for the unknowns at the moving interface. Of these equations, 2(C+1)-1 are species balances, and 1 is an enthalpy balance. Also, the saturations and mole fractions in the liquid hydrocarbon and vapour phases must sum to unity on both sides of the interface. In addition, since the steam front is at vapour-liquid equilibrium, there is an additional constraint to account for this. Hence, the total number of equations available at the moving interface is 2(C+1)+5.

3.3 The Modified Finite-Difference Formulation

3.3.1 Finite-Difference Form of the Matching Conditions

The selection of a finite-difference approximation for the matching conditions and the governing equations in the vicinity of a steam front is not as straight-forward as one might expect. It is well-known [11,12] that for convection-diffusion-type equations, there are finite-difference approximations which theoretically are quite accurate according to a standard error analysis, but which yield physically unrealistic or unstable solutions. In the present case, we found that a poor choice of a finite-difference approximation for the equations in the vicinity of a steam front may lead to problems similar to those discussed by Crichlow[11], and by Aziz and Settari[12].

The finite-difference approximation which we finally settled on is based on the assumption that the saturations and other quantities are gradually varying functions on either side of the front. There are, however, major variations from one side of the front to the other. Hence, it is reasonable to make the approximations

$$S_p^- \doteq S_{p,m-1}$$

$$S_p^+ \doteq S_{p,m+1}$$

where m denotes the moving grid point at the front (and X_m is set equal to X_B). Therefore, the finite-difference approximation to equation (3.7) can be written as

$$\{(\phi S_p \rho_p w_i)^n_{m-1} - (\phi S_p \rho_p w_i)^n_{m+1}\} V^n_f$$

$$= (T_p w_i)^n_{m+\frac{1}{2}}(P^n_{m+1}-P^n_m) - (T_p w_i)^n_{m-\frac{1}{2}}(P^n_m-P^n_{m-1}) + \sigma_p \overline{M}^n_i \qquad (3.9)$$

where

$$V^n_f = \frac{X^n_m - X^{n-1}_m}{\delta t} \qquad (3.10)$$

In equation (3.9), the subscripts $m+\frac{1}{2}$ and $m-\frac{1}{2}$ appear. Because of the discontinuities at the front, it is preferable to use the standard upstream-difference approximation instead of the mixed upstream-midstream-difference approximation which is used elsewhere in this simulator. Since we are assuming that the fluids are flowing from left to right, i.e. $P^n_{m-1} > P^n_m > P^n_{m+1}$, the standard upstream-difference approximation has the form

$$\left.\begin{aligned}(T_p w_i)^n_{m+\frac{1}{2}} &= \frac{(\tau_p w_i)^n_m}{X_{m+1}-X^n_m} \\ (T_p w_i)^n_{m-\frac{1}{2}} &= \frac{(\tau_p w_i)^n_{m-1}}{X^n_m - X_{m-1}}\end{aligned}\right\} \qquad (3.11)$$

The quantities $(\tau_p w_i)^n_m$ refer to a location at the front, on the downstream

side. Thus, the upstream-difference version of equation (3.9) is

$$\{(\phi S_p \rho_p w_i)_{m-1} - (\phi S_p \rho_p w_i)_{m+1}\} V_f$$

$$= (\tau_p w_i)_m \frac{P_{m+1}-P_m}{X_m - X_{m-1}} - (\tau_p w_i)_{m-1} \frac{P_m - P_{m-1}}{X_m - X_{m-1}} + \sigma_p \bar{M}_i \qquad (3.12)$$

(In equation (3.12), all variables are evaluated at time step n. Hence, superscripts have been omitted.) Likewise, the analogous finite-difference approximation for the enthalpy matching condition is

$$\{(\phi \sum_p S_p \rho_p h_p)_{m-1} - (\phi \sum_p S_p \rho_p h_p)_{m+1}\} V_f$$

$$+ \{((1-\phi)\rho_r h_r)_{m-1} - ((1-\phi)\rho_r h_r)_{m+1}\} V_f$$

$$= (\sum_p T_p h_p)_{m+\frac{1}{2}} (P_{m+1} - P_m) - (\sum_p T_p h_p)_{m-\frac{1}{2}} (P_m - P_{m-1})$$

$$+ (T_c)_{m+\frac{1}{2}} (T_{m+1} - T_m) - (T_c)_{m-\frac{1}{2}} (T_m - T_{m-1}) \qquad (3.13)$$

The total number of matching conditions at grid point m, which arise from equations (3.9) and (3.13), is identical to the number of balance equations in each grid block: namely 2(C+1). Hence, the moving grid point formulation fits in very neatly with the numerical procedure described in section 2. Furthermore, the number of unknowns to be determined at the moving grid point is also unchanged. On the side of the moving grid point where steam is present, pressure and temperature are related through equilibrium. Hence, only one of

pressure and temperature must be determined. The unknowns in this case are: $x_i, i=1,\ldots,C-1$, S_w, S_g and P or T.

At the moving grid point, pressure and temperature are still related by equilibrium. However, the gas saturation at this point is known to be zero. Hence, the unknowns in this case are: $x_i, i=1,\ldots,C-1$, S_w, P or T, and X_m.

On the side of the steam front without vapour, P and T are no longer coupled by equilibrium, but the gas saturation is still known to be zero. Hence, the unknowns in this case are: $x_i, i=1,\ldots,C-1$, S_w, P, and T.

3.3.2 The Downstream Grid Block

In our formulation, the finite-difference approximation to the governing equations downstream from the steam front (i.e. at $j=m+1$) is almost the same as it would be if there were no front-tracking. The main difference is that the control volume is taken to extend from $X=X_{m+1\frac{1}{2}}$ to the steam front $X=X_m^n$. (If there were no front-tracking, the control volume would extend from $X=X_{m+1\frac{1}{2}}$ to $X=X_{m+\frac{1}{2}}$.) In particular, the control volume neither changes in dimensions, nor contains the steam front during the time step. As a result, the finite-difference balance equations are

$$\frac{1}{\delta t}\,\delta(\phi S_p \rho_p w_i)^n_{m+1} = \frac{1}{X_{m+1\frac{1}{2}} - X_m^n}\,\Delta_x(T_p w_i \Delta_x P)^n_{m+1}$$

$$+ \sigma_p (M_i)^n_{m+1}\ ,$$

$$i=1,\ldots,C+1 \qquad (3.14)$$

and

$$\frac{1}{\delta t}\,\delta(\phi\,\Sigma_p S_p\rho_p h_p + (1-\phi)\rho_r h_r)^n_{m+1}$$

$$= \frac{1}{X_{m+1\frac{1}{2}}-X^n_m}\,\Delta_x(\Sigma_p T_p h_p \Delta_x P)^n_{m+1}$$

$$+ \frac{1}{X_{m+1\frac{1}{2}}-X^n_m}\,\Delta_x(T_c\Delta_x T)^n_{m+1} - (q_L)^n_{m+1} \qquad (3.15)$$

and do not contain any explicit dependence on the velocity of the front. Note that in equations (3.14) and (3.15), the variable X_m has a superscript denoting the time step.

3.3.3 The Upstream Grid Block

In our formulation, the finite-difference approximation to the governing equations upstream from the steam front (i.e. at j=m-1) is considerably different from what it would be if there were no front-tracking. One difference is that the control volume is taken to extend from $X=X_{m-1\frac{1}{2}}$ to the steam front $X=X^n_m$. (If there were no front-tracking, the control volume would extend from $X=X_{m-1\frac{1}{2}}$ to $X=X_{m-\frac{1}{2}}$.) This control volume includes a section of the reservoir between $X=X^{n-1}_m$ and $X=X^n_m$ which in the previous time step belonged to a different control volume. This fact requires the use of more complicated finite-difference equations.

$$\frac{X_m^{n-1}-X_{m-1\frac{1}{2}}}{X_m^n-X_{m-1\frac{1}{2}}}\frac{1}{\delta t}\,\delta(\phi S_p\rho_p w_i)_{m-1}^n$$

$$+\frac{X_m^n-X_m^{n-1}}{X_m^n-X_{m-1\frac{1}{2}}}\frac{1}{\delta t}\left[(\phi S_p\rho_p w_i)_{m-1}^n-(\phi S_p\rho_p w_i)_{m+1}^{n-1}\right]$$

$$=\frac{1}{X_m^n-X_{m-1\frac{1}{2}}}\left[(T_p w_i)_{m+\frac{1}{2}}^n(P_{m+1}^n-P_m^n)-(T_p w_i)_{m-1\frac{1}{2}}^n(P_{m-1}^n-P_{m-2}^n)\right]$$

$$+\sigma_p(M_i)_{m-1}^n\quad,\quad i=1,\ldots,C+1 \tag{3.16}$$

and

$$\frac{X_m^{n-1}-X_{m-1\frac{1}{2}}}{X_m^n-X_{m-1\frac{1}{2}}}\frac{1}{\delta t}\,\delta\Big(\phi\sum_p S_p\rho_p h_p+(1-\phi)\rho_r h_r\Big)_{m-1}^n$$

$$+\frac{X_m^n-X_m^{n-1}}{X_m^n-X_{m-1\frac{1}{2}}}\frac{1}{\delta t}\left[\Big(\phi\sum_p S_p\rho_p h_p+(1-\phi)\rho_r h_r\Big)_{m-1}^n-\Big(\phi\sum_p S_p\rho_p h_p+(1-\phi)\rho_r h_r\Big)_{m+1}^{n-1}\right]$$

$$=\frac{1}{X_m^n-X_{m-1\frac{1}{2}}}\left[\Big(\sum_p T_p h_p\Big)_{m+\frac{1}{2}}^n(P_{m+1}^n-P_m^n)-\Big(\sum_p T_p h_p\Big)_{m-1\frac{1}{2}}^n(P_{m-1}^n-P_{m-2}^n)\right]$$

$$+\frac{1}{X_m^n-X_{m-1\frac{1}{2}}}\left[(T_c)_{m+\frac{1}{2}}^n(T_{m+1}^n-T_m^n)-(T_c)_{m-1\frac{1}{2}}^n(T_{m-1}^n-T_{m-2}^n)\right]-(q_L)_{m-1}^n \tag{3.17}$$

where $(T_p)_{m+\frac{1}{2}}$ is defined as in (3.11), and the other $T_{j\pm\frac{1}{2}}$ are defined the same as for the non-front-tracking case.

A problem with equations (3.16) and (3.17) is that they depend on the pressures at four different grid points, i.e. P_{m-2}, P_{m-1}, P_m, and P_{m+1}. From a computational point of view, it is desirable to work with equations containing unknowns at only three grid points, namely m-2, m-1 and m. The simplest way to achieve this is to lag the pressures and other variables at grid point m+1 wherever they occur in the equations for the m-1 grid block. Since lagging any pressure is much more likely to cause numerical instability than lagging some of the other unknowns, it was decided to eliminate P^n_{m+1} by substituting the matching conditions (3.9) and (3.13) into (3.16) and (3.17) respectively. The resulting finite-difference equations are

$$\frac{X^{n-1}_m - X_{m-1\frac{1}{2}}}{X^n_m - X_{m-1\frac{1}{2}}} \frac{1}{\delta t}\, \delta(\phi S_p \rho_p w_i)^n_{m-1}$$

$$+ \frac{X^n_m - X^{n-1}_m}{X^n_m - X_{m-1\frac{1}{2}}} \frac{1}{\delta t}\left[(\phi S_p \rho_p w_i)^n_{m-1} - (\phi S_p \rho_p w_i)^{n-1}_{m+1}\right]$$

$$= \frac{1}{X^n_m - X_{m-1\frac{1}{2}}} \left[(T_p w_i)^n_{m-\frac{1}{2}}(P^n_m - P^n_{m-1}) - \sigma_p \overline{M_i}^n\right.$$

$$+\left\{(\phi S_p \rho_p w_i)^n_{m-1} - (\phi S_p \rho_p w_i)^n_{m+1}\right\} V^n_f$$

$$\left. - (T_p w_i)^n_{m-1\frac{1}{2}}(P^n_{m-1} - P^n_{m-2})\right]$$

$$+ \sigma_p (M_i)^n_{m-1}\,, \quad i=1,\ldots,C+1 \qquad (3.18)$$

for the molar balances, and

$$\frac{X_m^{n-1}-X_{m-1\frac{1}{2}}}{X_m^n-X_{m-1\frac{1}{2}}}\frac{1}{\delta t}\,\delta(\phi\,\textstyle\sum_p S_p\rho_p h_p + (1-\phi)\rho_r h_r)_{m-1}^n$$

$$+\frac{X_m^n-X_m^{n-1}}{X_m^n-X_{m-1\frac{1}{2}}}\frac{1}{\delta t}\left[(\phi\,\textstyle\sum_p S_p\rho_p h_p+(1-\phi)\rho_r h_r)_{m-1}^n - (\phi\,\textstyle\sum_p S_p\rho_p h_p+(1-\phi)\rho_r h_r)_{m+1}^{n-1}\right]$$

$$=\frac{1}{X_m^n-X_{m-1\frac{1}{2}}}\{\,(\textstyle\sum_p T_p h_p)_{m-\frac{1}{2}}^n(P_m^n-P_{m-1}^n) - (\textstyle\sum_p T_p h_p)_{m-1\frac{1}{2}}^n(P_{m-1}^n-P_{m-2}^n)$$

$$+\,(T_c)_{m-\frac{1}{2}}^n(T_m^n-T_{m-1}^n) - (T_c)_{m-1\frac{1}{2}}(T_{m-1}^n-T_{m-2}^n)$$

$$+\left[(\phi\textstyle\sum_p S_p\rho_p h_p)_{m-1}^n - (\phi\textstyle\sum_p S_p\rho_p h_p)_{m+1}^n\right] V_f^n$$

$$+\left[((1-\phi)\rho_r h_r)_{m-1}^n - ((1-\phi)\rho_r h_r)_{m+1}^n\right] V_f^n\} - (q_L)_{m-1}^n \qquad (3.19)$$

for the enthalpy balance.

3.3.4 Overtaking a Stationary Grid Point

The finite-difference approximations derived in the previous sections are valid provided that the moving grid point does not overtake a stationary grid point during the time step. If the moving grid point does overtake a

stationary grid point, then, since a reordering of the grid points occurs, some changes must be made to the terms which have the superscript n-1.

The matching conditions (3.9) and (3.13) do not require any change because they contain no terms with the superscript n-1. However, it is necessary to modify the equation for the front velocity V_f^n to

$$V_f^n = \frac{X_m^n - X_{m-1}^{n-1}}{\delta t} \tag{3.20}$$

The balance equations (3.14) and (3.15) for the downstream grid block contain one term which must be modified, namely $\delta(\xi)_{m+1}^n$, where ξ is either $\phi S_p \rho_p w_i$ or $\phi \sum_p S_p \rho_p h_p + (1-\phi)\rho_r h_r$. Since $\delta(\xi)_{m+1}^n$ denotes the change, during the time step, of the average value of ξ in a <u>fixed</u> region downstream from the front, $\delta(\xi)_{m+1}^n$ should be replaced with

$$(\xi)_{m+1}^n - \frac{X_{m+1\frac{1}{2}} - X_{m+\frac{1}{2}}^{n-1}}{X_{m+1\frac{1}{2}} - X_m^n} (\xi)_{m+1}^{n-1} - \frac{X_{m+\frac{1}{2}}^{n-1} - X_m^n}{X_{m+1\frac{1}{2}} - X_m^n} (\xi)_m^{n-1}$$

where the second and third terms of this expression are a weighted average of ξ at time step n-1. (Since $X_{m+1\frac{1}{2}}$ is the location of a stationary grid point, no superscript is required for $X_{m+1\frac{1}{2}}$.) Therefore, the modified molar balance equations for the downstream grid block are

$$\frac{1}{\delta t}\{(\phi S_p \rho_p w_i)^n_{m+1} - \frac{X_{m+1\frac{1}{2}} - X^{n-1}_{m+\frac{1}{2}}}{X_{m+1\frac{1}{2}} - X^n_m}(\phi S_p \rho_p w_i)^{n-1}_{m+1}$$

$$- \frac{X^{n-1}_{m+\frac{1}{2}} - X^n_m}{X_{m+1\frac{1}{2}} - X^n_m}(\phi S_p \rho_p w_i)^{n-1}_m\} \qquad (3.21)$$

$$= \text{right-hand-side of equation (3.14)}$$

and the modified enthalpy balance equation for the downstream grid block is

$$\frac{1}{\delta t}\{(\phi \sum_p S_p \rho_p h_p + (1-\phi)\rho_r h_r)^n_{m+1}$$

$$- \frac{X_{m+1\frac{1}{2}} - X^{n-1}_{m+\frac{1}{2}}}{X_{m+1\frac{1}{2}} - X^n_m}(\phi \sum_p S_p \rho_p h_p + (1-\phi)\rho_r h_r)^{n-1}_{m+1}$$

$$- \frac{X^{n-1}_{m+\frac{1}{2}} - X^n_m}{X_{m+1\frac{1}{2}} - X^n_m}(\phi \sum_p S_p \rho_p h_p + (1-\phi)\rho_r h_r)^{n-1}_m\}$$

$$= \text{right-hand-side of equation (3.15)} \qquad (3.22)$$

The balance equations for the upstream grid block, i.e. (3.16) and (3.17), and (3.18) and (3.19), contain four types of terms which must be modified: V^n_f, X^{n-1}_m, $\delta(\xi)^n_{m-1}$, and $(\xi)^{n-1}_{m+1}$, where ξ is either $\phi S_p \rho_p w_i$ or $\phi \sum_p S_p \rho_p h_p + (1-\phi)\rho_r h_r$. V^n_f should be redefined as in equation (3.20). Since, in equations (3.18) and

(3.19), X_m^{n-1} denotes the former location of the front, X_m^{n-1} should be replaced with X_{m-1}^{n-1}. Since, in equations (3.18) and (3.19), $\delta(\xi)_{m-1}^n$ denotes the change in the value of ξ upstream from the front, $\delta(\xi)_{m-1}^n$ should be replaced with $(\xi)_{m-1}^n-(\xi)_{m-2}^{n-1}$. Finally, since $(\xi)_{m+1}^{n-1}$ denotes the value of ξ downstream from the front, it should be replaced with $(\xi)_m^{n-1}$. Therefore, the modified molar balance equations for the upstream grid block are

$$\frac{X_{m-1}^{n-1}-X_{m-1\frac{1}{2}}}{X_m^n-X_{m-1\frac{1}{2}}}\frac{1}{\delta t}\left[(\phi S_p\rho_p w_i)_{m-1}^n-(\phi S_p\rho_p w_i)_{m-2}^{n-1}\right]$$

$$+\frac{X_m^n-X_{m-1}^{n-1}}{X_m^n-X_{m-1\frac{1}{2}}}\frac{1}{\delta t}\left[(\phi S_p\rho_p w_i)_{m-1}^n-(\phi S_p\rho_p w_i)_m^{n-1}\right]$$

$$=\text{right-hand-side of (3.18)} \qquad (3.23)$$

where V_f^n is defined in (3.20), and the modified enthalpy balance equation for the upstream grid block is

$$\frac{X_{m-1}^{n-1}-X_{m-1\frac{1}{2}}}{X_m^n-X_{m-1\frac{1}{2}}}\frac{1}{\delta t}\left[(\phi\sum_p S_p\rho_p h_p+(1-\phi)\rho_r h_r)_{m-1}^n-(\phi\sum_p S_p\rho_p h_p+(1-\phi)\rho_r h_r)_{m-2}^{n-1}\right]$$

$$+\frac{X_m^n-X_{m-1}^{n-1}}{X_m^n-X_{m-1\frac{1}{2}}}\frac{1}{\delta t}\left[(\phi\sum_p S_p\rho_p h_p+(1-\phi)\rho_r h_r)_{m-1}^n-(\phi\sum_p S_p\rho_p h_p+(1-\phi)\rho_r h_r)_m^{n-1}\right]$$

$$=\text{right-hand-side of (3.19)} \qquad (3.24)$$

3.4 The Solution Method

The proposed iterative method is similar to the method used to solve the equations for the non-front-tracking case. The variables and equations are split into two groups as in table 3.2.

Table 3.2 Interaction Variables and Equations - Front-Tracking

PT variables	P_j^n	T_j^n	X_m^n	$(S_g)_j^n$	$(q_T)_j^n$	TOTAL
# of variables	$N-N_G-2$	$N-1$	1	N_G	2	2N

SX Variables	$(S_w)_j^n$	$(S_o)_j^n$	$(x_i)_j^n$	TOTAL
# of variables	N	0	$(C-1)N$	CN

PT equations	(2.19)	(2.22)	(2.23)	(3.25)	(3.26)	(3.27)	(3.28)	TOTAL
# of equations	N-3	N-3	0	2	2	1	1	2N

SX equations	(2.26)	(2.27)	(3.29)	(3.30)	(3.33)	TOTAL
# of equations	$(C-1)(N-3)$	N-3	$2(C-1)$	3	C-1	CN

The rest of the discussion in section 2.3 applies to the front-tracking case as well as to the non-front-tracking case.

3.4.1 The PT Equations

In section 2.3, it was shown how equations (2.19) and (2.22) were derived from the non-front-tracking governing equations (2.1) and (2.2) for the reservoir. The same procedure was applied to the front-tracking system of equations (2.1) and (2.2) with matching conditions (3.9) and (3.13), and modified balance equations (3.14), (3.15), (3.18), and (3.19). Since the governing equations for the front-tracking case are the same as for the non-front-tracking case for all grid points except those in the immediate vicinity of the front, equations (2.19) and (2.22) are applicable for all grid points except j=m-1, m and m+1. In addition, the method used to derive equations (2.19) and (2.22) is applicable also to the balance equations (3.14), (3.15), (3.18) and (3.19) for grid points m-1 and m+1, although these equations are different in form from (2.1) and (2.2). It would be possible to write out the resulting equations for grid points m-1 and m+1 in a form analogous to that of (2.19) and (2.22). However, we neither derived nor used the equations in such a form. Instead, it is more convenient to express the rearranged equations as

$$\frac{1}{(\rho_w)_j^n}\left[(F_{BLw})_j^n + (F_{BVw})_j^n\right] + \frac{1}{(\rho_{o,1})_j^n}\left[(F_{BL1})_j^n + (F_{BV1})_j^n\right]$$

$$+ \frac{1}{(\rho_{o,2})_j^n}\left[(F_{BL2})_j^n + (F_{BV2})_j^n\right] + \frac{1}{(\rho_{o,3})_j^n}(F_{BL3})_j^n = 0 \ ,$$

$$j=m-1,m+1 \qquad (3.25)$$

and

$$(h_w)_j^n[(F_{BLw})_j^n + (F_{BVw})_j^n] + (h_{o,1})_j^n[F_{BL1})_j^n + (F_{BV1})_j^n]$$

$$+ (h_{o,2})_j^n [(F_{BL2})_j^n + (F_{BV2})_j^n] + (h_{o,3})_j^n(F_{BL3})_j^n$$

$$- (F_{BH})_j^n = 0 \ , \ j=m-1,m+1 \qquad (3.26)$$

where

$$(F_{BLi})_j^n = 0 \ , \ i=w,1,2,3$$

is the molar balance equation ((3.18) for j=m-1 or (3.14) for j=m+1) for component i in the liquid phase,

$$(F_{BVi})_j^n = 0 \ , \ i=s,1,2$$

is the molar balance equation ((3.18) for j=m-1 or (3.14) for j=m+1) for component i in the vapour phase, and

$$(F_{BH})_j^n = 0$$

is the total enthalpy balance equation ((3.19) for j=m-1 or (3.15) for j=m+1).

Although it is possible to use the same procedure to combine the matching conditions as was used to combine the balance equations (for $j \neq m$), the result would be a pair of equations in which the influence of the front velocity is very small. This result would be desirable in the SX equations, but is not desirable in the PT equations. Instead, it is preferable to maintain the influence of the front velocity, and to decrease the influence of the liquid-phase saturations S_w and S_o, e.g. on the $(\Delta_x T_p w_i \Delta_x P)_{m+\frac{1}{2}}$ terms. The PT equations for grid point m, which are used in the simulator, are

$$-\left(\frac{dk_{ro}}{dS_w}\right)_m^n \left(\frac{\mu_w}{\rho_w}\right)_m^n \left[(F_{BLw})_m^n + (F_{BVw})_m^n\right]$$

$$+ \left(\frac{dk_{rw}}{dS_w}\right)_m^n \left(\frac{\mu_o}{\rho_{o,1}}\right)_m^n \left[(F_{BL1})_m^n + (F_{BV1})_m^n\right]$$

$$+ \left(\frac{dk_{rw}}{dS_w}\right)_m^n \left(\frac{\mu_o}{\rho_{o,2}}\right)_m^n \left[(F_{BL2})_m^n + (F_{BV2})_m^n\right]$$

$$+ \left(\frac{dk_{rw}}{dS_w}\right)_m^n \left(\frac{\mu_o}{\rho_{o,3}}\right)_m^n (F_{BL3})_m^n = 0 \qquad (3.27)$$

and

$$(h_w)_{m-1}^n \left[(F_{BLw})_m^n + (F_{BVw})_m^n\right] + (h_{o,1})_{m-1}^n \left[(F_{BL1})_m^n + (F_{BV1})_m^n\right]$$

$$+ (h_{o,2})_{m-1}^n \left[(F_{BL2})_m^n + (F_{BV2})_m^n\right] + (h_{o,3})_{m-1}^n (F_{BL3})_m^n - (F_{BH})_m^n = 0 \quad (3.28)$$

Since the condensation terms drop out of the sums

$$(F_{BLw})_j^n + (F_{BVw})_j^n \text{ , } (F_{BL1})_j^n + (F_{BV1})_j^n \text{ , and } (F_{BL2})_j^n + (F_{BV2})_j^n,$$

there is no need to discuss modifications or analogues of equation (2.23).

3.4.2 The SX Equations

Section (2.4) explains why the set of liquid-phase mole balances is over-determined, and shows how the redundancy can be eliminated by replacing two of the mole balances with a linear combination selected so that the iteration procedure converges quickly. The same technique was applied to the

front-tracking set of equations. However, the linear combinations which are used are different. Thus, the equations which are used to solve for the SX variables in the grid blocks adjacent to the front, i.e. $j=m\pm1$, are

$$(F_{BLi})_j^n + (F_{BVi})_j^n = 0 \ , \ i=1,\ldots,C-1 \ , \ j=m-1,m+1 \tag{3.29}$$

and

$$(\bar{\lambda}_{C+1})_j^n (F_{BLC})_j^n - (\bar{\lambda}_C)_j^n [(F_{BLw})_j^n + (F_{BVw})_j^n] = 0 \ ,$$

$$j=m-1,m,m+1 \tag{3.30}$$

where

$$\left.\begin{aligned} (\bar{\lambda}_{C+1})_{m-1}^n &= \frac{2(\tau_w)_{m-1}^n}{X_m^n - X_{m-1}} + \frac{(\tau_w)_{m-1\frac{1}{2}}^n}{X_{m-1} - X_{m-2}} \\ (\bar{\lambda}_{C+1})_{m+1}^n &= \frac{2(\tau_w)_{m+1\frac{1}{2}}^n}{X_{m+2} - X_{m+1}} + \frac{(\tau_w)_m^n}{X_{m+1} - X_m^n} \end{aligned}\right\} \tag{3.31}$$

and

$$(\bar{\lambda}_C)_{m-1}^n = \frac{2(\tau_o x_C)_{m-1}^n}{X_m^n - X_{m-1}} + \frac{(\tau_o x_C)_{m-1\frac{1}{2}}^n}{X_{m-1} - X_{m-2}} \tag{3.32a}$$

$$(\bar{\lambda}_C)^n_{m+1} = \frac{2(\tau_o x_C)^n_{m+1\frac{1}{2}}}{X_{m+2}-X_{m+1}} + \frac{(\tau_o x_C)^n_m}{X_{m+1}-X^n_m} \tag{3.32b}$$

and $(\bar{\lambda}_C)^n_m$ and $(\bar{\lambda}_{C+1})^n_m$ are defined in equations (3.34) and (3.35).

(In our simulator, C, the number of components in the liquid hydrocarbon phase, is set to 3. It is assumed that at least one of the hydrocarbon components is non-volatile, and can be assigned, without loss of generality, the subscript C.)

A different set of linear combinations are used to solve for the SX variables at the front, i.e. at j=m. These equations are

$$[(\phi S_o \rho_o x_C)^n_{m-1} - (\phi S_o \rho_o x_C)^n_{m+1}][(F_{BLi})^n_m + (F_{BVi})^n_m]$$

$$-0.9999[(\phi S_o \rho_o x_i + \phi S_g \rho_g y_i)^n_{m-1} - (\phi S_o \rho_o x_i + \phi S_g \rho_g y_i)^n_{m+1}](F_{BLC})^n_m = 0 \ , \ i=1,\ldots,C-1 \tag{3.33}$$

and (3.30), (with j=m)

where

$$(\bar{\lambda}_{C+1})^n_m = \frac{(\tau_w)^n_m}{X_{m+1}-X^n_m} \tag{3.34}$$

and

$$(\bar{\lambda}_C)_m^n = \frac{(\tau_o x_C)_m^n}{X_{m+1}^n - X_m^n} \qquad (3.35)$$

3.5 Results and Discussion

3.5.1 Injection Rate

A primary reason for incorporating a front-tracking feature into our reservoir simulator is to eliminate spurious fluctuations in the steam injection rate as a function of time, and to calculate the steam injection rate with better accuracy. Figures 3.4 and 3.5 illustrate the effectiveness of the front-tracking modifications in this regard. If the front-tracking modifications are not used, then the calculated injection rate repeatedly drops suddenly by a factor of 3 to 5, as figure 3.4 shows, and recovers slowly, only to drop again suddenly by a similar amount. The times at which these sudden drops occur coincide with the times at which vapour begins collecting in a grid block in which all of the incoming vapour was condensing during previous time steps. (A similar effect can be observed in figure 3 of a paper by Vinsome[9], reproduced as figure 1.1 in this report.) On the other hand, if the front-tracking modifications are used, then, as figure 3.5 shows, the fluctuations in the injection rate are reduced considerably in magnitude and are shorter-lived. Therefore, the front-tracking modifications are successful in fulfilling the purpose for which they were introduced.

3.5.2 Cumulative Injection

One interesting observation which one might make about figures 3.4 and 3.5 is that the simulated steam injection process, according to the simulation as depicted in figure 3.4, appears to be occurring significantly more quickly than

the same steam injection process, as depicted in figure 3.5. In other words, the time of the recovery process predicted by the simulation is affected significantly by the choice of the finite-difference method. This observation implies that either the front-tracking method or the non-front-tracking method, or both methods, possesses a significant error due to the finite-differencing procedure. Indeed, sizable truncation errors have been reported (for a non-front-tracking method) by Abou-Kassem and Aziz[13], who have concluded that the time/pore-volume-injected (PVI) relationship is very sensitive to the grid size.

For the purpose of studying the discretization error, the same steam injection process was simulated both with and without front-tracking, for four different grid sizes (i.e. a distance of 68.2 m was divided into 5, 10, 17, and 25 blocks, respectively), and plots of the cumulative amount of the steam-water mixture injected as a function of time were constructed. These plots are shown in figures 3.6 and 3.7. These plots show: (i) that the fluctuations in the injection rate apparent in figures 3.4 and 3.5 are almost eliminated by the process of integrating the injection rate to obtain the amount injected; and (ii) that the cumulative amount of steam-water mixture injected is very sensitive to the grid size.

For each simulation, the time required to inject 0.3 pore volumes (cold-water-equivalents) of the steam-water mixture was calculated and plotted in figure 3.8. Figure 3.8 shows that, both with front-tracking and without front-tracking, the calculated injection time is very sensitive to the grid size. Since for fine grids, the truncation error for the finite-difference method with upstream differencing is roughly proportional to the width of one grid block[12], and since the abscissa of the plot in figure 3.8 is a quantity proportional to the width of one grid block (i.e. it is the width of one grid

block divided by 68.2 metres), it is reasonable to extrapolate the curves in figure 3.8 to infinitesimally fine grids, (i.e. $\Delta X \to 0$). If this is done, the extrapolated curves intersect near the $\Delta X=0$ axis. This indicates that the injection times calculated by the front-tracking method and by the non-front-tracking method both converge to the same answer for fine grids. Therefore, the discrepancies among the eight calculated times may be attributed to truncation errors and/or numerical dispersion.

Although the truncation error for both methods is large, the truncation error of the front-tracking method is significantly smaller than the error of the non-front-tracking method. This improvement is not surprising because the front-tracking method calculates the injection rate more accurately and, as will be pointed out in subsequent discussion, suppresses some numerical dispersion.

Although the front-tracking modifications have resulted in a smaller truncation error, the error is still large enough to cause concern. The curves in figure 3.8 indicate that when two-dimensional simulations are performed, large numbers of grid points will be required in order to attain acceptable accuracy. A clue to the nature of this large error is shown in figure 3.9. For the purpose of calculating the cumulative amounts injected, shown in figure 3.9, the simulations were repeated, but with one difference: the viscosities of the vapour, water and hydrocarbon phases were set to the constant values of 10^{-5}, 5×10^{-4} and 10^{-1} Pa sec. respectively, instead of being described as functions of temperature. A comparison of figures 3.7 and 3.9 shows that this one change in the simulation causes a dramatic reduction in the sensitivity of the average injection rate to the size of the grid. Although the modified viscosities are quite unrealistic (if the viscosities do not depend on temperature, there is not much point in injecting steam into the reservoir),

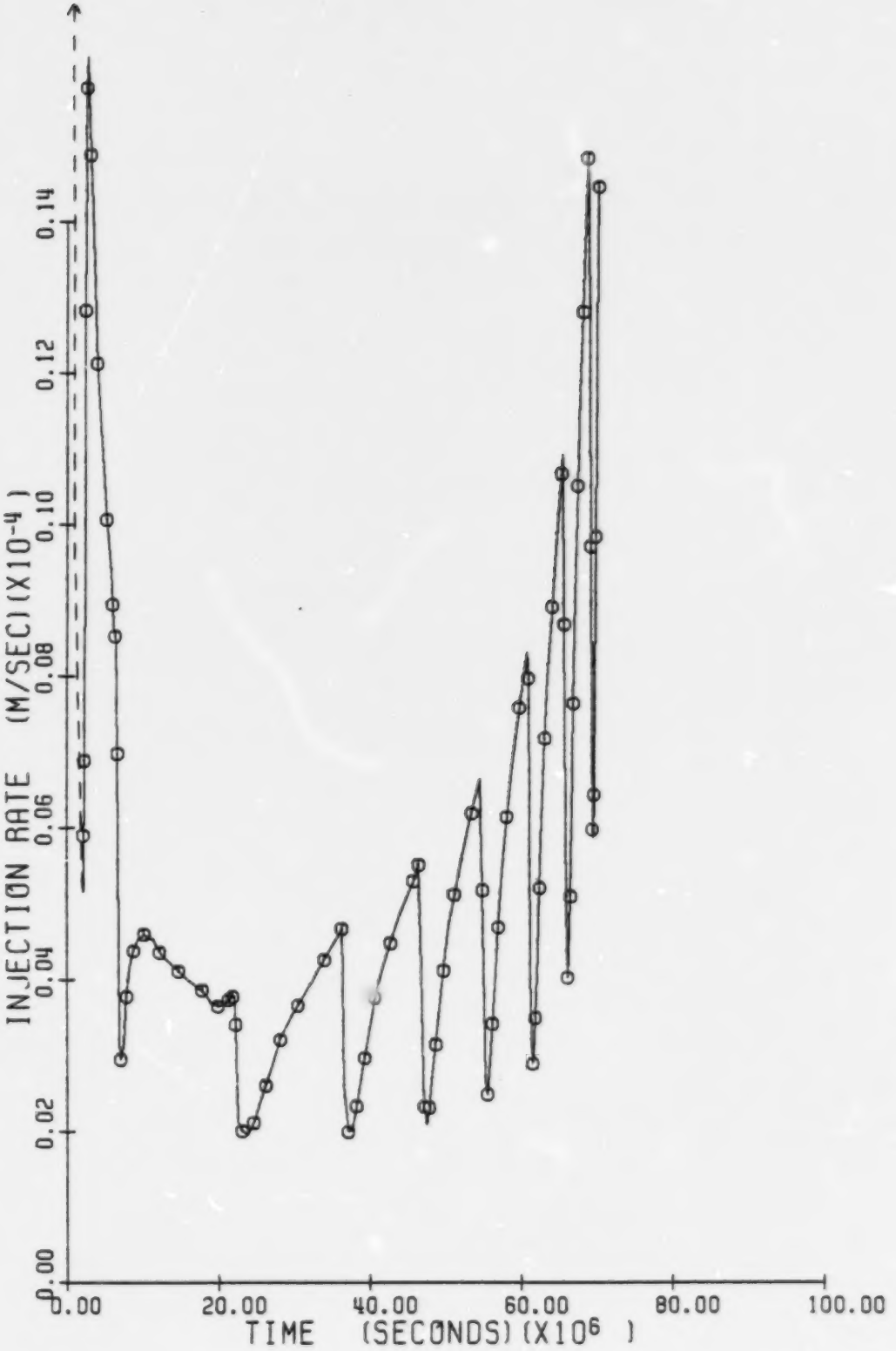

Figure 3.4 - Injection rate calculated without front-tracking (17 grid blocks)

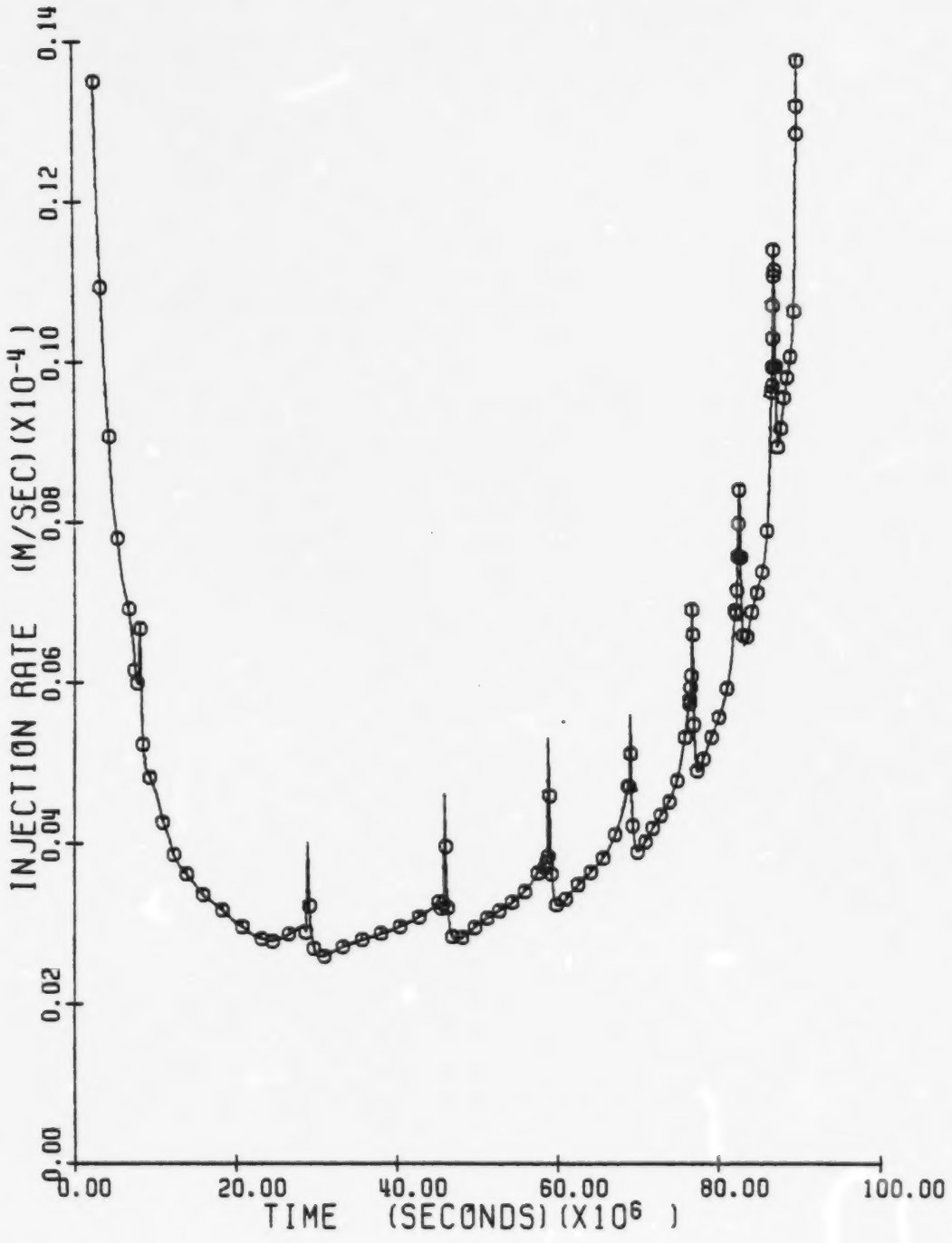

Figure 3.5 - Injection rate calculated using front-tracking (17 grid blocks)

this comparison does suggest that the truncation error is linked in some way to the calculated temperature distribution in the reservoir. This insight offers some hope for finding a way to reduce the discretization error of the simulator.

3.5.3 Profiles

Plots of temperature, pressure, the three phase saturations, and the composition of the hydrocarbon phase as a function of position are shown in figures 3.10,3.11,3.12, and 3.13. These plots were obtained for two simulations, one with front-tracking and one without front-tracking, on a grid with 17 grid blocks, and describe the profiles of the six variables after 0.3 pore volumes (cold-water-equivalent) of the steam-water mixture have been injected.

The pressure profile is flat not only in the region in which vapour is present, but also in a large part of the region in which no vapour is present. This implies that the pressure gradient depends less on the relative permeabilities of the three phases, and more on the viscosity of the oil phase. The pressure profiles resulting from the front-tracking simulation and the non-front-tracking simulation (figures 3.11 and 3.10 respectively) are practically identical.

The temperature profile is flat in the region in which vapour is present, but drops moderately sharply downstream from the front. There are strong theoretical grounds for attributing the lack of a sharp thermal front to a combination of numerical dispersion (induced by the finite-differencing scheme) and thermal conduction. In the absence of some form of conduction, a sharp thermal front should result. It is our conclusion that it is the rate of advance of the thermal "wave" that controls the rate of advance of the steam front, and hence the rate of steam injection. For the larger grid

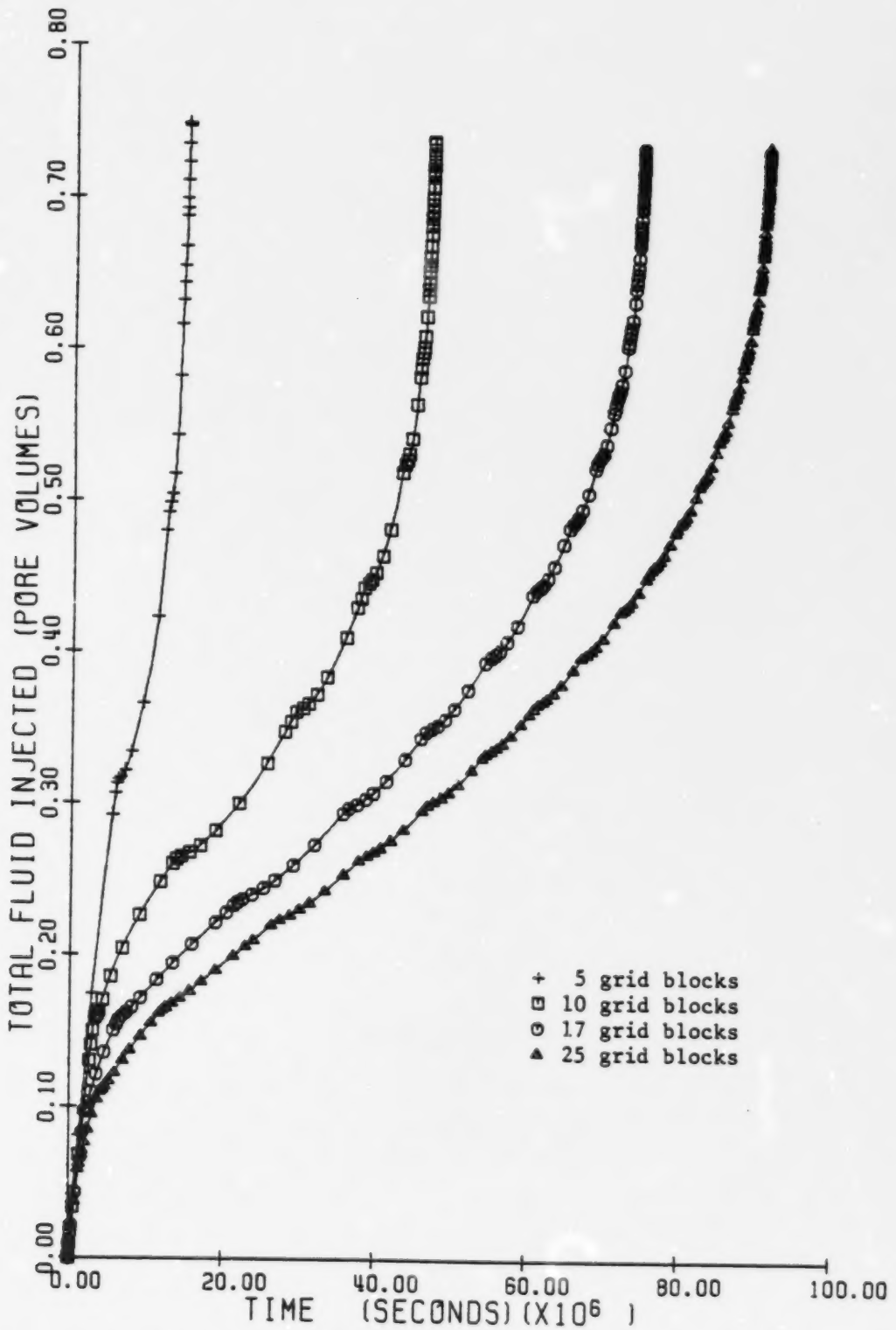

Figure 3.6 - Grid-size dependence of cumulative injection (without front-tracking)

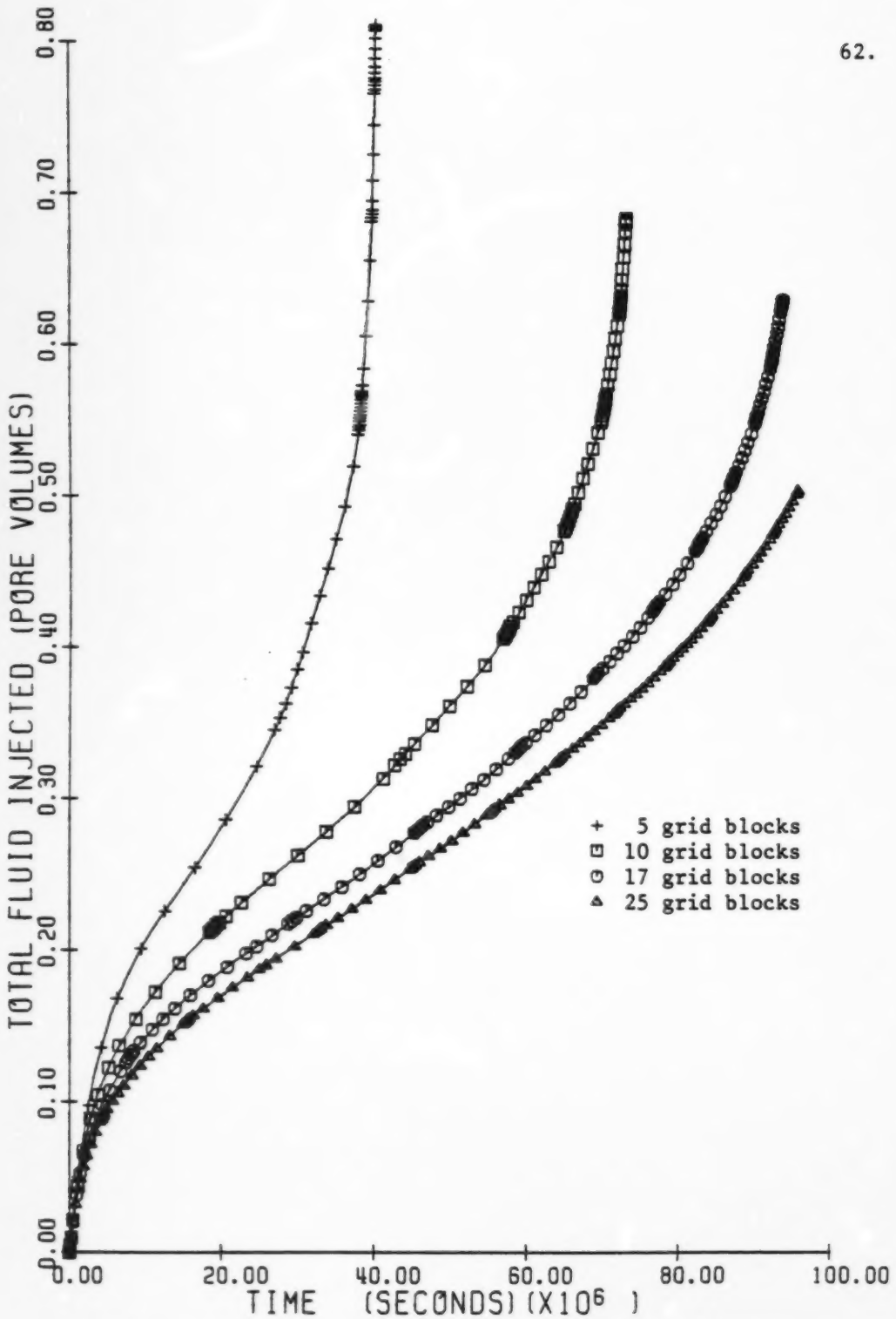

Figure 3.7 - Grid-size dependence of cumulative injection (with front-tracking)

spacings, numerical dispersion is greater and, as a consequence, the thermal wave travels more rapidly than it does for small grid spacings. Ultimately, the rate of advance of the steam front and the rate of steam injection will be higher for the larger grid spacing. This conclusion is also supported by the observation that profiles of temperature, pressure and saturations are not strongly affected by grid spacing, provided that profiles for different grid sizes are compared at different times with the same cumulative injection. (However, the times required to achieve these similar profiles are strong functions of grid size.) A comparison of figures 3.10 and 3.11 shows a 25% discrepancy in the times required for front-tracking and non-front-tracking simulations to achieve 0.3 PVI. Since numerical dispersion increases the simulated rate of steam injection, this suggests that the front-tracking formulation is less dispersive.

The plots of the three phase saturations and the hydrocarbon composition (figures 3.12 and 3.13) show significant differences between the two simulations. The front-tracking simulation predicts sharper fronts, especially for the hydrocarbon composition and the hydrocarbon phase saturations. The front-tracking simulation predicts relatively flat profiles upstream from the steam front, whereas the non-front-tracking simulation predicts a boundary layer in the vicinity of the injection face, and also predicts some spurious-looking undulations in the interior of the region in which vapour is present. However, the most significant difference between the saturation profiles in figures 3.12 and 3.13 is in the oil phase saturation upstream from the steam front. The front-tracking simulation predicts that during the first phase of a steamflood (prior to breakthrough), the oil saturation upstream from the steam

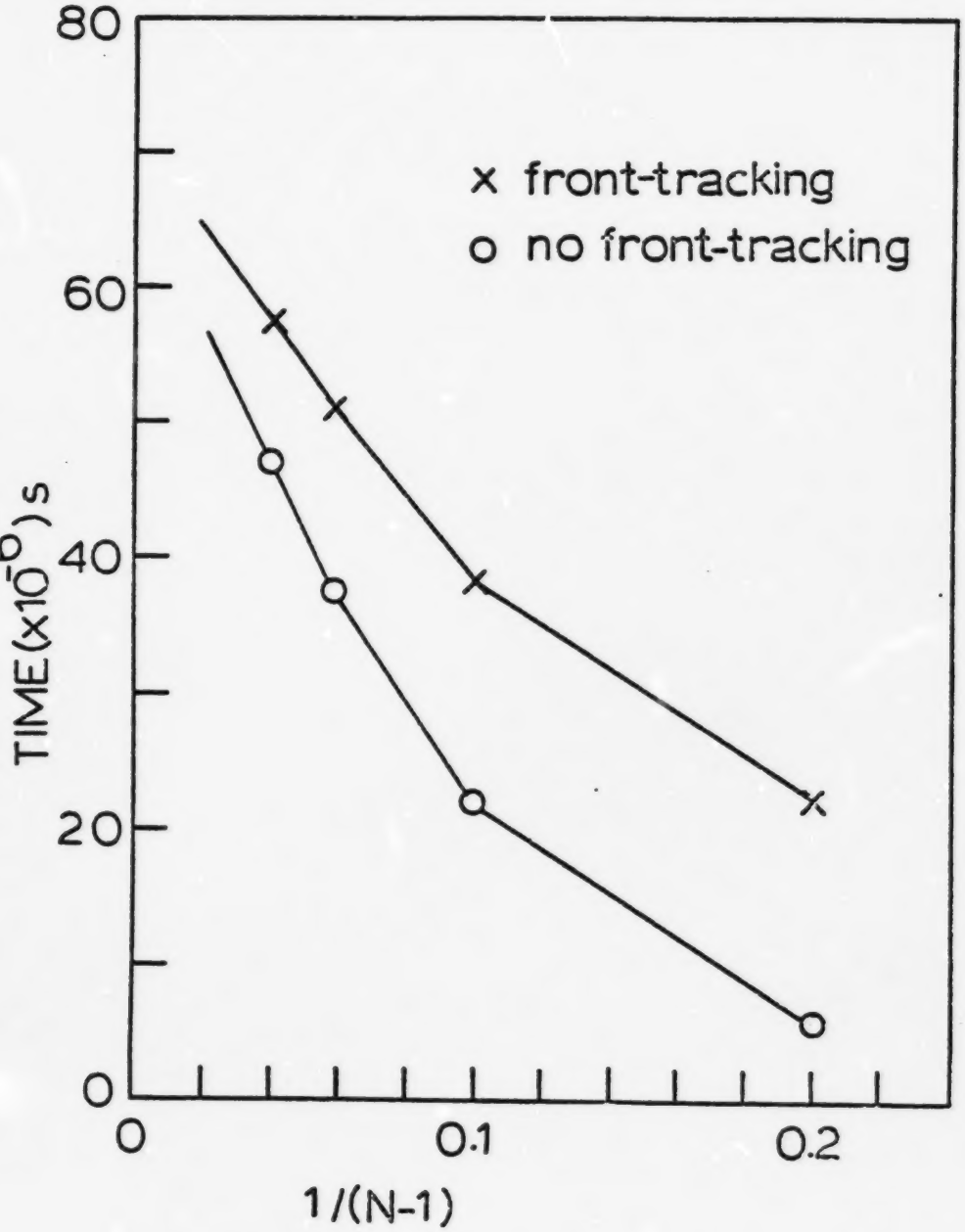

Figure 3.8 - Time required to inject 0.3 pore volumes as a function of grid size

front is reduced to near residual, but as the steam front advances, it leaves behind it a little more oil in each grid block than it did in the preceding grid block. This implies that during a steamflood, most of the oil is produced before the steam front "breaks through" to the production face. The non-front-tracking simulation, on the other hand, predicts that the oil saturation upstream from the steam front is significantly larger than the residual saturation. Thus, a significant fraction of the oil is left to be produced after the steam front breaks through. It is not obvious which version of the simulator provides the most accurate prediction in this regard.

3.5.4 Material and Enthalpy Balances

Significant (up to 24%) material balance errors have been reported[1] for a simulator which is similar to the one discussed in the present work. To the contrary, we have found that the material and enthalpy balance errors are generally less than 10^{-2}%, and, hence, negligible.

3.5.5 Computation Time

The convergence of the two-level iteration method is fast but variable. The mean number of iterations per time step required by the two-level method for three problems is shown in table 3.3. Problem #1 is the test problem described in section 2 of this report. Problem #2 is the same as problem #1, except that the viscosities of the vapour, water, and hydrocarbon phases have been set to the constant values of 10^{-5}, 5×10^{-4}, and 10^{-1} Pa•s respectively. Problem #3 is the same as problem #1, except that the mole fraction of volatile oil in the hydrocarbon phase has been set to zero. Except for problem #3, the front-tracking version of the simulator requires approximately the same number of iterations per time step for convergence. This is somewhat disappointing, because we had hoped that the front-tracking modification would reduce the

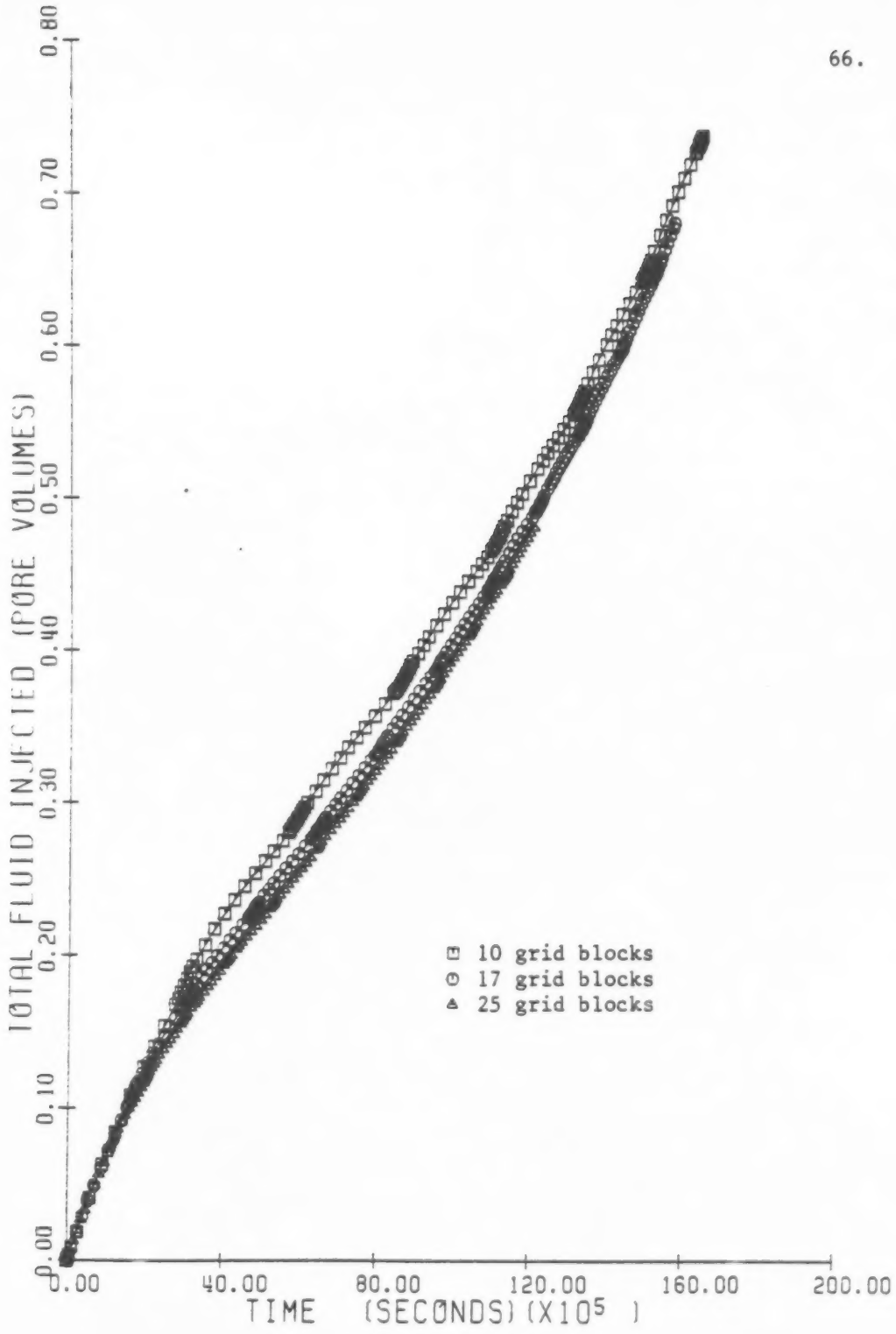

Figure 3.9 - Grid-size dependence of cumulative injection for a constant-viscosity simulation (with front-tracking)

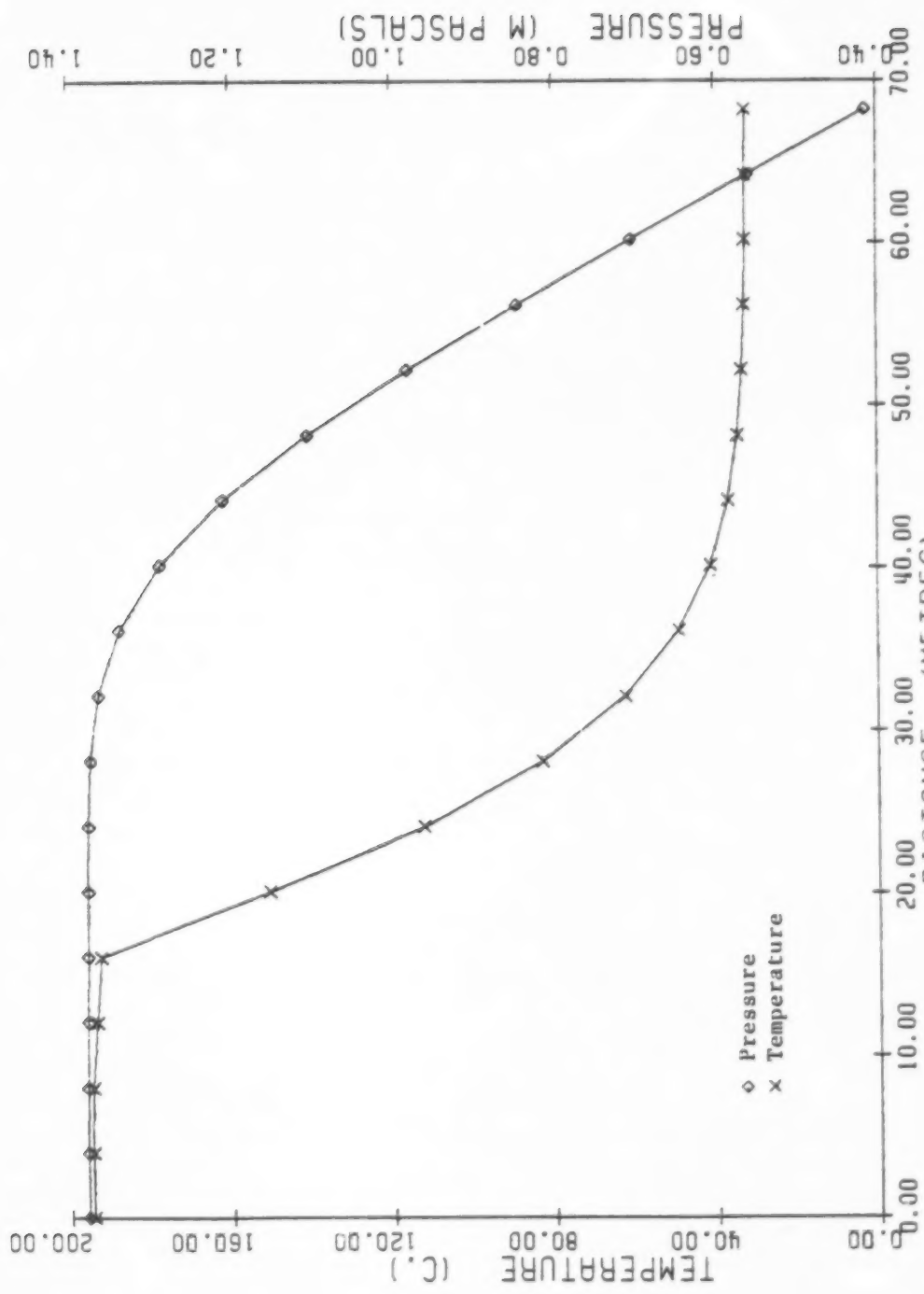

Figure 3.10 - Pressure and temperature profiles after 0.3 pore volumes were injected (37,600,000 sec., no front-tracking, 17 grid blocks)

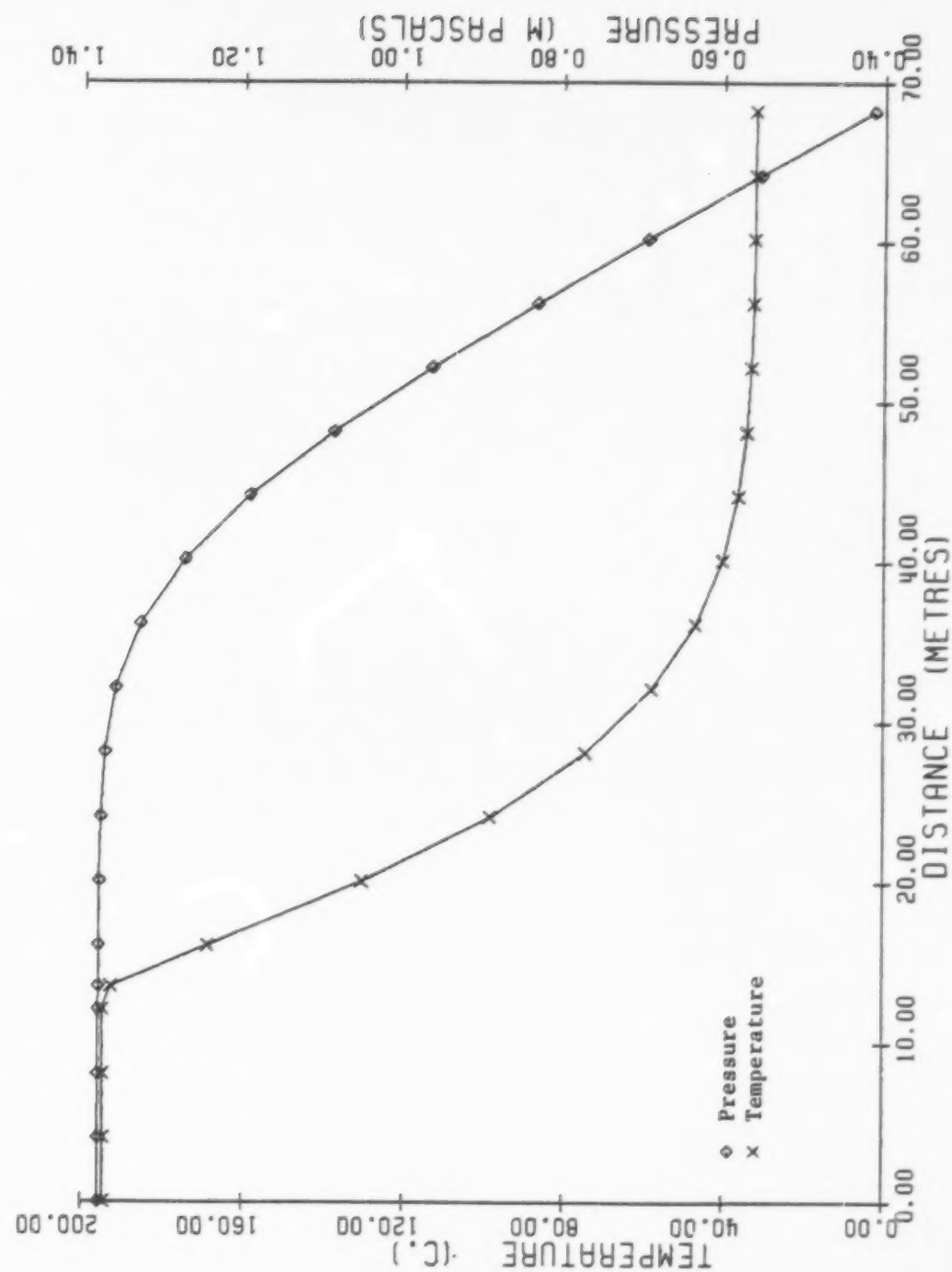

Figure 3.11 - Pressure and temperature profiles after 0.3 pore volumes were injected (50,500,000 sec., front-tracking, 17 grid blocks)

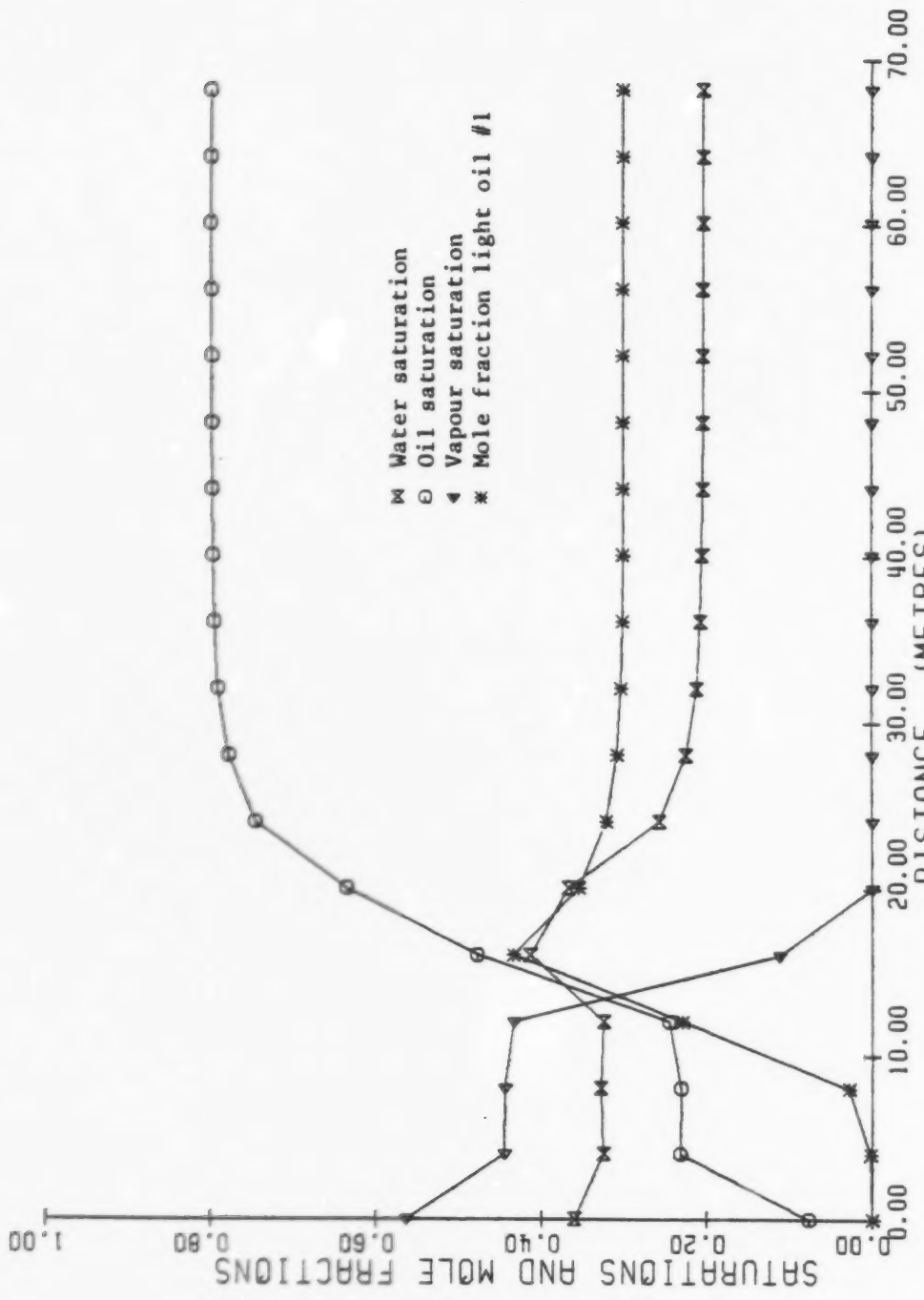

Figure 3.12 - Saturation and composition profiles after 0.3 pore volumes were injected (37,600,000 sec., no front-tracking, 17 grid blocks)

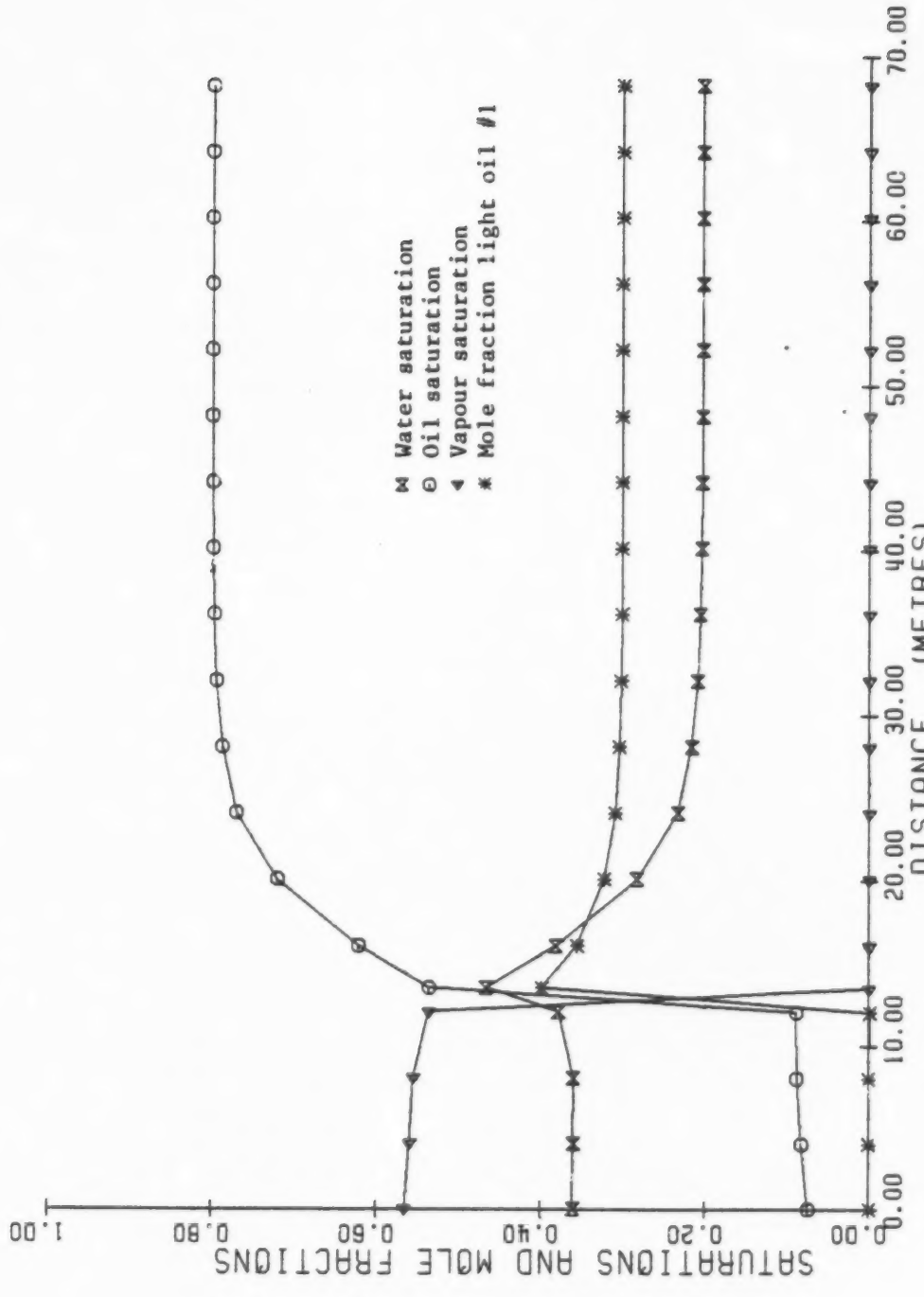

Figure 3.13 - Saturation and composition profiles after 0.3 pore volumes were injected (50,500,000 sec., front-tracking, 17 grid blocks)

number of iterations required. The relatively poor performance of the front-tracking version for problem #3 is unexplained at this point in time.

The front-tracking modification also requires more than 1½ times as much computation time per time step as would be required if the simulator were run without front-tracking. Most of this extra computation time, however, can be attributed to the use of a numerically calculated Jacobian in the vinicity of the moving grid point,

Table 3.3 - Numerical Performance of Simulator for the Test Problems

Problem No.	number of blocks	front-tracking	mean number of iterations	computation time (ms/block step)
1	17	No	5.1	37
1	17	Yes	6.1	67
1	25	No	5.1	36
1	25	Yes	6.7	62
2	17	No	10.9	73
2	17	Yes	11.1	117
3	17	No	8.2	55
3	17	Yes	18.0	176

and could be reduced somewhat if the Jacobian were calculated analytically. The computation time can also be reduced if the Jacobian is not

calculated every iteration. Although the results discussed in this report were obtained by recalculating the Jacobian every iteration, we have found that the number of iterations required per time step is increased only marginally if the Jacobian is calculated only on the first iteration, and on every fifth iteration thereafter. However, the reliability of the simulator decreases drastically if this is done.

Not only does the number of iterations per time step vary between problems, but it also varies within a single simulation. In each simulation, several time steps required at least 4 more than the mean number of iterations, and, sometimes, the iteration method failed to converge even in 29 iterations. Thus, the convergence of the iteration method is rather variable.

Not only is the convergence of the iteration method variable, but the reliability of the simulator has been less than desirable, especially when the Jacobian is not recalculated every iteration. Although the simulator is capable of performing successfully calculations for hundreds of time steps in a row, it frequently quits before the steam front has passed through half of the grid blocks. This problem is aggravated if the Jacobian is evaluated only once every five iterations. However, the reliability of the simulator can definitely be increased to an acceptable level with a relatively small amount of additional work. It should be noted that the simulator is always reliable if the front-tracking option is not used, and the Jacobian is evaluated at every iteration.

4. CONCLUSIONS

The two-level implicit technique for simulating oil recovery by steam injection has been discussed in some detail, and it has been demonstrated in section 2 to be a viable alternative to the fully implicit approach for one-dimensional problems.

In section 3, a numerical procedure for tracking the location of the steam front was presented and implemented in the two-level iterative scheme. A comparison of solutions obtained with, and without, front-tracking demonstrated several advantages of the front-tracking approach including:

(i) reduction of spurious injection rate variations as the steam front advances, and

(ii) smaller discretization error.

Our comparison of the two simulators has led us to the conclusion that the discretization error of steam injection simulators is due primarily to numerical dispersion of the temperature.

Essential to the success of the two-level method is the use of the $\bar{\lambda}$-factors, as discussed in sections 2.4 and 3.4, which very effectively reduce the coupling between the two levels of the iteration procedure. The number of available $\bar{\lambda}$-factors does not increase as the spatial dimensionality of the problem increases. On the other hand, the number of flux terms in the finite-difference equations does increase as the spatial dimensionality of the problem increases. Since it is the purpose of the $\bar{\lambda}$-factors to reduce the interactions caused by these flux terms, we anticipate that this decoupling technique will be considerably less effective for two-and three-dimensional simulations. Hence, the two-level method appears to be considerably less promising for two- and three-dimensional problems than previously anticipated. In the interest of developing a front-tracking simulator in two dimensions, it is therefore prudent to defer the further development of the two-level approach and to adopt, instead, a fully implicit scheme for front-tracking in two dimensions.

ACKNOWLEDGEMENT

The constant-pressure-adjusted-temperature method, discussed in pages 19 and 20 of this report, arose out of discussions during a visit by one of us (PGdB) to the Computer Modelling Group, Calgary, Alberta.

NOMENCLATURE

Finite Difference Operators

$\delta(\xi)_j^n \equiv (\xi)_j^n - (\xi)_j^{n-1}$

$\Delta_X(T\eta\Delta_X\xi)_j^n \equiv (T\eta)_{j+\frac{1}{2}}^n(\xi_{j+1}^n-\xi_j^n) - (T\eta)_{j-\frac{1}{2}}^n(\xi_j^n-\xi_{j-1}^n)$

Variables

B	half the number of boundary grid points
C	number of components in the oil phase
D_4	the computation time reduction factor if D4 ordering is used
F_{BH}	an abbreviation for the discretized enthalpy balance
F_{BLi}	an abbreviation for the discretized material balance for component i in a liquid phase
F_{BVi}	an abbreviation for the discretized material balance for component i in the vapour phase
f_{Dw}	an estimate of $-(S_w^n-S_w^{(n,k-1)})/(S_g^{(n,k)}-S_g^{(n,k-1)})$, defined in equation (2.24) and explained in the text which precedes (2.24)
$\underset{\sim}{F}_{PT}$	vector of PT equations
$\underset{\sim}{F}_{SX}$	vector of SX equations
h	molar enthalpy
$J^{(n,m)}$	Jacobian matrix
J_p	injected flow fraction $J_p(0,t) = \dfrac{q_p(0,t)}{q_T(0,t)}$
k	absolute permeability
k_r	relative permeability

M	condensation rate
$\overline{M}$	strength of a condensation point source
N	number of grid points
N_G	number of grid points with vapour
o	According to the standard terminology of asymptotic analysis (e.g. de Bruijn[14]), the expression $f(x) = o(\phi(x))$ means that as x tends to 0, the ratio $f(x)/\phi(x)$ tends to zero. Little "o" should not be confused with big "O", which has a different standard meaning.
P	pressure
P_i	pure oil component vapour pressure
P_s	water vapour pressure
q	volumetric flow rate
q_L	rate of heat loss
S	saturation
T	temperature (Celsius)
t	time
U	generalized system variable (P, T, S, x)
$\underset{\sim}{U}_{PT}$	vector of PT unknowns
$\underset{\sim}{U}_{SX}$	vector of SX unknowns
V_f	velocity of the steam front
w	mole fraction, liquid or vapour phase
X	distance
X_B	location of the steam front
x	mole fraction, liquid phase
y	mole fraction, vapour phase
δt	time step

η an arbitrary variable

λ mobility

$\bar{\lambda}$ factors defined in equations (2.25), (2.26), (3.31), (3.32), (3.34) and (3.35)

μ viscosity

ξ an arbitrary variable

ρ density

σ sign of condensation term: $\sigma_g = -1$, $\sigma_o = \sigma_w = +1$

τ transmissibility: $\tau = kk_r\rho/\mu$

T scaled transmissibility: $(T_p)^n_{j\pm\frac{1}{2}} = (\tau_p)^n_{j\pm\frac{1}{2}}/\pm(X_{j\pm1}-X_j)$

T_c scaled transmissibility of heat due to heat conduction

ϕ porosity

Subscripts

g vapour phase

i any component, never a grid point index

j grid point index

ℓ any liquid phase

m the moving grid point

o hydrocarbon (oil) phase

p any phase

r rock

s steam

T total over all three phases

up($j+\frac{1}{2}$) the grid point upstream from $j+\frac{1}{2}$

w water phase

Superscripts

k	iteration
n	time step
-	the negative side of the interface
+	the positive side of the interface

REFERENCES

1. Coats, K.H., "A Highly Implicit Steamflood Model", Soc. Pet. Eng. J., 18, 369-383 (1978).
2. Gottfried, B.S., "A Mathematical Model of Thermal Oil Recovery in Linear Systems", Soc. Pet. Eng. J., 5, 196-210 (1965).
3. Shutler, N.D., "Numerical, Three-Phase Simulation of the Linear Steamflood Process", Soc. Pet. Eng. J., 9, 232-246 (1969).
4. Shutler, N.D., "Numerical Three-Phase Model of the Two-Dimensional Steamflood Process", Soc. Pet. Eng. J., 10, 405-417 (1970).
5. Adler, G., "A Linear Model and a Related Very Stable Numerical Method for Thermal Secondary Oil Recovery", J. Cdn. Pet. Tech., 14(3), 56-65 (1975).
6. El-Khatib, N.A.F. and Fulton, P.F., "Factors Affecting Oil Recovery by Forward In Situ Combustion", paper presented at the 29th C.S.Ch.E. Conference, Sarnia, Ont., Sept. 30-Oct. 3, 1979.
7. Beattie, C.I., "Numerical Simulation of Oil Recovery by Steam Injection", M.A.Sc. Thesis, University of Toronto, 1980.
8. Coats, K.H., "Simulation of Steamflooding with Distillation and Solution Gas", Soc. Pet. Eng. J., 16, 235-247 (1976).

9. Vinsome, P.K.W., "A Numerical Description of Hot-Water and Steam Drives by the Finite-Difference Method", paper SPE 5248 presented at the 49th SPE-AIME Annual Fall Meeting, Houston, Texas, Oct. 6-9, 1974.

10. Fong, F.K. and Skidmore, D.R., "Combined ADI Iteration and Implicit Central Difference Numerical Method for Solving Nonlinear Conjugated Partial Differential Equations with Moving Boundary Heat Transfer in In-Situ Coal Liquefaction", Advances in Computer Methods for Partial Differential Equations III, eds. Vichnevetsky, Stepleman, 1979, pp. 120-126.

11. Crichlow, H.B., "Modern Reservoir Engineering - A Simulation Approach", (Prentice-Hall, Englewood Cliffs, NJ, 1977), chapters 4,5.

12. Aziz, K. and Settari, A., "Petroleum Reservoir Simulation", (Applied Science Publishers, Ltd., London, 1979), chapters 3,5.

13. Abou-Kassem, J.H. and Aziz, K., "Sensitivity of Steamflood Model Results to Grid and Timestep Sizes", Soc. Pet. Eng. J., 24, 65-74 (1984).

14. de Bruijn, N.G., "Asymptotic Methods in Analysis", (Dover edition, Dover, New York, 1981), chapter 1.

APPENDIX - FLUID AND RESERVOIR PROPERTIES

All quantities have the standard SI units with two sets of exceptions:

1) the unit of temperature is Celsius degrees

2) the unit of mass is the kg mol for the densities, enthalpies, and transmissibilities

The properties were chosen so that our test problem would be similar to the second test problem considered in Coats' paper.

Vapour pressures

Vapour pressure of water:

$$p_s(T) = 2.92356 \times 10^{-4}\, T^{4.226015}$$

Vapour pressure of hydrocarbon component #1:

$$p_1(T) = 2.095250 \times 10^{9} \times 10^{-[1745.38/(T+230.00)]}$$

Vapour pressures of hydrocarbon component #2:

$$p_2(T) = 1.072877 \times 10^{9} \times 10^{-[1211.03/(T+220.79)]}$$

Vapour pressure of hydrocarbon component #3:

$$p_3(T) = 0$$

Total vapour pressure:

$$P(T) = p_s(T) + \sum_{i=1}^{3} x_i p_i(T)$$

Vapour Phase Mole Fractions

Mole fraction of steam at a grid point:

$$(y_s)_j = \frac{p_s(T_j)}{P(T_j)}$$

Mole fraction of a hydrocarbon component at a grid point:

$$(y_i)_j = \frac{(x_i)_j p_s(T_j)}{P(T_j)}$$

Mole fraction of steam between grid points:

$$(y_s)_{j+\frac{1}{2}} = \frac{p_s(T_{j+\frac{1}{2}})}{p_s(T_{j+\frac{1}{2}}) + \sum_{i=1}^{3}(x_i)_{up(j+\frac{1}{2})} p_i(T_{j+\frac{1}{2}})}$$

where $T_{j+\frac{1}{2}} = \frac{1}{2}(T_j + T_{j+1})$

Mole fraction of a hydrocarbon component between grid points:

$$(y_i)_{j+\frac{1}{2}} = \frac{(x_i)_{up,(j+\frac{1}{2})} p_i(T_{j+\frac{1}{2}})}{p_s(T_{j+\frac{1}{2}}) + \sum_{i=1}^{3}(x_i)_{up(j+\frac{1}{2})} p_i(T_{j+\frac{1}{2}})}$$

where $T_{j+\frac{1}{2}} = \frac{1}{2}(T_j + T_{j+1})$

Heat Loss

$q_L = 0$

Enthalpies

For this section, T_a is defined by $T_a = \frac{1}{2}(T+12.8)$

Enthalpy of the liquid water phase:

$$h_w = T\{75273.14 + 2.131292\ T_a - 0.03704971\ T_a^2 + 0.0001746477\ T_a^3\}$$

Enthalpy of hydrocarbon #1 in the liquid hydrocarbon phase:

$$h_{o1} = 251160\ T$$

Enthalpy of hydrocarbon #2 in the liquid hydrocarbon phase:

$$h_{o2} = T\{62591 + 233.627(T_a + 273.15)\}$$

Enthalpy of hydrocarbon #3 in the liquid hydrocarbon phase:

$$h_{o3} = 627900\ T$$

Enthalpy of the liquid hydrocarbon phase:

$$h_o = x_1 h_{o1} + x_2 h_{o2} + x_3 h_{o3}$$

Enthalpy of steam in the vapour phase:

$$h_{gs} = 4.507907 \times 10^7 + 18.02\ T \{1832.89 + 0.7443\ T_a - 0.00011240\ T_a^2\}$$

Enthalpy of hydrocarbon #1 in the vapour phase:

$$h_{g1} = 4.7129 \times 10^6 + 120\ T \{2104.73 + 3.6967\ T_a - 0.00013383\ T_a^2 - 5.4428 \times 10^{-7}\ T_a^3\}$$

Enthalpy of hydrocarbon #2 in the vapour phase:

$$h_{g2} = 3.4823 \times 10^{-7} + 78.11\ T \{948.74 + 4.2211\ T_a - 0.0032279\ T_a^2 + 9.9377 \times 10^7\ T_a^3\}$$

Enthalpy of the vapour phase:

$$h_g = h_{gs} y_s + h_{g1} y_1 + h_{g2} y_2$$

Volumetric enthalpy of the rock (Joules/m^3K, not J/kg mol K):

$$p_r h_r = 2.35 \times 10^6 \times \frac{1 - 0.38000 \times 0.99993}{1 - \phi}$$

Enthalpy between grid blocks:

$$(h_p)_{j+\frac{1}{2}} = (h_p)_{up(j+\frac{1}{2})}$$

Thermal Conductivity

$$k_c = 2.09$$

Transmissibility of heat due to heat conduction:

$$(T_c)_{j+\frac{1}{2}} = \frac{(k_c)_{up(j+\frac{1}{2})}}{X_{j+1} - X_j}$$

Densities

Density of the liquid water phase:

$$\rho_w = 55.5\ (1.024 - 7.4 \times 10^{-4}\ T + 4.5 \times 10^{-10}\ P)$$

Density of the vapour phase (The ideal gas law is used):

$$\rho_g = \frac{1.202726 \times 10^{-4}\ P}{T + 273.15}$$

Density of hydrocarbon component #1:

$$\rho_{o1} = 6.93\ (1 - 7.4 \times 10^{-4}\ (T - 32.2) + 7.3 \times 10^{-10}\ (P - 5.17 \times 10^{7}))$$

Density of hydrocarbon component #2:

$$\rho_{o2} = \left[12.143 - 6.7853 \times 10^{-3} \times [1.8\ T + 32] - \frac{230.444}{620.6 - [1.8\ T + 32]}\right] \times \left[1 + 1.3 \times 10^{-9}\ (P - 101325)\right]$$

Density of hydrocarbon component #3:

$$\rho_{o3} = 2.77\ (1 - 7.4 \times 10^{-4}\ (T - 32.2) + 7.3 \times 10^{-10}\ (P - 5.17 \times 10^{7}))$$

Density of the liquid hydrocarbon phase:

$$\rho_o = \left[\frac{x_1}{\rho_{o1}} + \frac{x_2}{\rho_{o2}} + \frac{x_3}{\rho_{o3}}\right]^{-1}$$

Viscosities

The viscosities of the liquid water phase and of the vapour phase are calculated from table A1 by interpolating between the viscosities plotted as functions of the natural logarithm of the temperature measured in Kelvin degrees. The viscosity of the liquid hydrocarbon phase is given by the formula

$$\mu_o = \mu_{oT}(T)\ \mu_{ox}(x_3)$$

where $\mu_{oT}(T)$ is calculated from table A1 using linear interpolation between the values of $\mu_{oT}(T)$ plotted as a function of the natural logarithm of the temperature measured in Kelvin degrees, and $\mu_{ox}(x_3)$ is calculated from Table A2 by linear interpolation. (Both tables are the same as those given by Coats[1].) The units of μ_{oT} are Pa•s, and μ_{ox} is dimensionless.

Table A1 - Dependence of Viscosity on Temperature

T(°F)	$\mu_{oT}(T)$	μ_w	μ_g
75.0	5.7800	9.20×10^{-4}	0.095×10^{-4}
100.0	1.3800	6.81×10^{-4}	0.102×10^{-4}
150.0	0.1870	4.35×10^{-4}	0.115×10^{-4}
200.0	0.0470	3.05×10^{-4}	0.127×10^{-4}
250.0	0.0174	2.35×10^{-4}	0.138×10^{-4}
300.0	0.0085	1.87×10^{-4}	0.149×10^{-4}
350.0	0.0052	1.56×10^{-4}	0.158×10^{-4}
500.0	0.0025	1.18×10^{-4}	0.174×10^{-4}

Table A2 - Dependence of Liquid Hydrocarbon Viscosity on Composition

x_3	$\mu_{ox}(x_3)$
0.1667	0.25
0.5000	0.35
0.6670	0.50
0.7500	1.00
0.8571	2.50
1.0000	6.00

Relative Permeabilities

The relative permeability to the liquid water phase, k_{rw}, is calculated from table A3 using linear interpolation. The relative permeability to the vapour phase, k_{rg}, is calculated from table A4 using linear interpolation. The relative permeability to the liquid hydrocarbon phase is calculated from Stone's 3-phase formula for relative permeability (Coats[1])

$$k_{ro} = (k_{row} + k_{rw})(k_{rog} + k_{rg}) - k_{rw} - k_{rg}$$

where k_{rw} and k_{row} are calculated from table A3, and k_{rg} and k_{rog} are calculated from table A4, using linear interpolation. If the formula produces a value for k_{ro} which is less than 0, then k_{ro} is set to 0.

Absolute Permeability

$k = 3.948 \times 10^{-12}\ m^2$

Porosity

$\phi = 0.38000\ (0.99993 + 7 \times 10^{-10}\ P)$

Table A3 - Dependence of Relative Permeabilities on the Liquid Water Phase Saturation

S_w	k_{rw}	k_{row}
0.200	0.0000	1.0000
0.250	0.0102	0.7690
0.294	0.0168	0.7241
0.357	0.0275	0.6206
0.414	0.0424	0.5040
0.490	0.0665	0.3714
0.557	0.0970	0.3029
0.630	0.1148	0.1555
0.673	0.1259	0.0956
0.719	0.1381	0.0576
0.789	0.1636	0.0000
1.000	0.2500	0.0000

Table A4 - Dependence of Relative Permeabilities on the Vapour Phase Saturation

S_g	k_{rg}	k_{rog}
0	0.0000	1.0000
10^{-5}	0.0000	1.0000
0.101	0.0026	0.5169
0.150	0.0121	0.3373
0.195	0.0195	0.2919
0.250	0.0285	0.2255
0.281	0.0372	0.2170
0.337	0.0500	0.1764
0.386	0.0654	0.1433
0.431	0.0761	0.1172
0.485	0.0855	0.0883
0.567	0.1022	0.0461
0.605	0.1120	0.0294
0.710	0.1700	0.0000

Mobilities

The mobilities at the grid points are calculated from the formula

$$(\lambda_p)_j = \frac{k(k_{rp})_j}{(\mu_p)_j}$$

The mobilities halfway between grid points are calculated from the formula

$$(\lambda_p)_{j+\frac{1}{2}} = \frac{2k(k_{rp})_{up(j+\frac{1}{2})}}{(\mu_p)_j + (\mu_p)_{j+1}}$$

Transmissibilities

The transmissibilities at the grid points are calculated from the formula

$$(\tau_p)_j = k(k_{rp})_j \frac{(\rho_p)_j}{(\mu_p)_j}$$

The transmissibilities halfway between grid points are calculated from the formula

$$(\tau_p)_{j+\frac{1}{2}} = k(k_{rp})_{up(j+\frac{1}{2})} \frac{(\rho_p)_j + (\rho_p)_{j+1}}{(\mu_p)_j + (\mu_p)_{j+1}}$$

The scaled transmissibilities T_p are related to the transmissibilities by the formula

$$(T_p)_{j+\frac{1}{2}} = \frac{(\tau_p)_{j+\frac{1}{2}}}{X_{j+1}-X_j}$$